OPTIMIZATION OF STRONTIUM ALUMINATE PHOSPHOR FOR DEVELOPMENT OF A COLLOIDAL NANOPARTICLE INK SOLUTION

A Report of a Senior Study

by

Alexandria Bone

Major: Chemistry

Maryville College

Spring, 2017

Date approved _____, by _____

Faculty Supervisor

Date approved _____, by _____

Division Chair

ABSTRACT

Strontium aluminate with Eu^{2+} and Dy^{3+} has been at the forefront of emerging applications for storage phosphors since its discovery in 1996. In this study, the emission intensity and luminescence lifetime of $SrAl_2O_4:Eu^{2+}$, Dy^{3+} were enhanced by partial substitution of Ca^{2+} into Sr^{2+} sites in the matrix. The most efficient host matrix, $Sr_{0.9}Ca_{0.1}Al_2O_4$, was further optimized for Eu^{2+} and Dy^{3+} dopant content, and the optimal Eu^{2+} to Dy^{3+} ratio was determined to be 6:1. The $Sr_{0.83}Ca_{0.1}Al_2O_4$:6 mol% Eu^{2+}, 1 mol% Dy^{3+} phosphor was then synthesized with varying concentrations of H_3BO_3 flux; the most efficient phosphor was synthesized with 20 mol% H_3BO_3. Physical characteristics, such as crystal structure and surface morphology, were examined by XRD and SEM. Optical characteristics, such as emission and excitation bands and the luminescence lifetime of the materials, were examined by spectrofluorometry as well as direct imaging of the phosphors. In order to develop a colloidal nanoparticle ink solution, future work must be carried out to decrease the particle size of the phosphor and provide more detailed characterization of the final phosphor material.

ACKNOWLEDGEMENTS

*This manuscript has been authored by UT-Battelle, LLC under Contract No. DE-AC05-00OR22725 with the U.S. Department of Energy. The United States Government retains and the publisher, by accepting the article for publication, acknowledges that the United States Government retains a non-exclusive, paid-up, irrevocable, world-wide license to publish or reproduce the published form of this manuscript, or allow others to do so, for United States Government purposes. The Department of Energy will provide public access to these results of federally sponsored research in accordance with the DOE Public Access Plan (*http://energy.gov/downloads/doe-public-access-plan*).*

Special thanks to Dr. Brenda Smith, Mr. Cyril Thompson, Dr. Linda Lewis, Dr. Brent Dial, and Mr. Cody Lekavich of Oak Ridge National Laboratory (ORNL) as well as Dr. Mary Turner of Maryville College for their generous help in the production of this work. Special thanks are also extended to the Higher Education Research Experiences program facilitated by the Oak Ridge Institute for Science and Education and the Applied Technologies Group of ORNL for making this work possible.

TABLE OF CONTENTS

LIST OF FIGURES

CHAPTER I

INTRODUCTION

BACKGROUND AND PROPERTIES OF PHOSPHOR MATERIALS

Introduction and Background

Luminescent materials emit light when they are excited by a non-thermal source such as electrical energy, mechanical stress, subatomic motion, or a chemical reaction.[1] Luminescence is divided into categories by excitation source: for example, luminescence by mechanical stress is mechanoluminescence, absorption of a photon results in photoluminescence, etc. Photoluminescence is subdivided by the duration of the detectable emission after excitation ends. *Storage phosphors* exhibit phosphorescence (also known as persistent luminescence), meaning they emit for an extended period of time—from seconds to tens of hours—after the excitation source is removed, whereas fluorescent materials only emit under active excitation or for nanoseconds afterwards.[2]

Photoluminescent materials are also classified according to the region(s) of the electromagnetic spectrum that they absorb and emit most efficiently. Many storage phosphors absorb ultraviolet (UV) light and emit in the visible range. These phosphors are particularly useful for a broad range of applications due to the widespread availability and low-cost of UV excitation sources (e.g., the sun) and the ease of emission detection by the human eye. Storage phosphors are currently utilized in safety indicators, traffic signage, solar

cells[3], fluorescent paints and inks[4], ceramics[5], and light-emitting diodes (LEDs).[1] Due to the relative novelty of storage phosphors to the scientific community, potential applications are under rapid development; these include uses in environmental dosimetry, electron beam operating devices[1], textile fibers, optical data storage[6], damage detection in bridges and buildings, decorative displays[7], fluorescent lamps, biomedical technology (e.g., *in vivo* medical imaging)[8,9], and more.

Although scientific advancement of storage phosphor technology has primarily emerged over the past twenty years, mankind has observed persistent luminescence for centuries. The first recognized natural phosphor—a diamond—was reported by Benvenuto Cellini in 1568.[10] The phosphorescent properties of certain diamonds were confirmed by Robert Boyle nearly 100 years later.[10] Circa 1602, Vincent Casciorolo discovered a barium sulfate that exhibited persistent luminescence after calcination; known as the "Bologna Stone," Casciorolo's material was the first "artificial" storage phosphor that could be reproducibly synthesized, and its discovery intrigued and perplexed many prominent seventeenth-century thinkers—most notably, Galileo.[10] Several studies on the Bologna phosphor emerged in the 1600s and 1700s, but the most significant work is arguably that of Jacopo Bartholomeo Beccari, professor of physics at the Institute of Sciences and Arts at Bologna. Beccari's prime focus was to determine the effects of excitation color, intensity, and duration on the resulting emission; he also discovered that many other inorganic and organic materials exhibit a luminescent afterglow.[10]

By the end of the nineteenth century, several other storage phosphors—mainly sulfides—had been synthesized and studied alongside the Bologna Stone. The most significant of these early storage phosphors is hexagonal zinc sulfide (ZnS), initially

discovered in 1866 by Theodor Sidot.[10] After subsequent studies proved that incorporating heavy metal impurities (i.e., dopants) could control and enhance phosphor emissions, Sidot's ZnS co-doped with copper and cobalt became the most prominent storage phosphor developed for application in the 1900s.[10] The green emission of ZnS:Cu,Co, centered at 530 nm, is ideal for practical applications because it is easily observed by the human eye. However, the luminescence lifetime of ZnS:Cu,Co only lasts for 2-3 hours[11], which severely limits its potential for commercial development. To remedy this, radioisotopes such as tritium and promethium were incorporated into ZnS:Cu,Co paints.[11] While this practice extends the phosphorescence of ZnS:Cu,Co, it also makes the material significantly more toxic to humans and the environment, again limiting its viability for widespread use.

Thus, until the 1990s, there was a dire need for a bright, long-lasting and non-toxic storage phosphor suitable for commercial applications. In 1996, Matsuzawa *et al.* answered this need with a strontium aluminate co-doped with europium and dysprosium ($SrAl_2O_4:Eu^{2+}$, Dy^{3+}), a storage phosphor with a bright green emission similar to that of ZnS:Cu,Co. The results of Matsuzawa's afterglow lifetime study are shown in Figure 1.

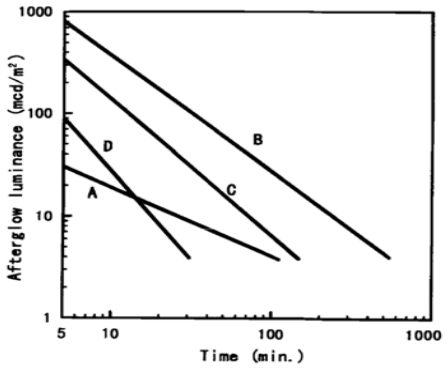

Figure 1. Phosphorescence characteristics of (A) $SrAl_2O_4:Eu^{2+}$, (B) $SrAl_2O_4:Eu^{2+}$, Dy^{3+}, (C) $SrAl_2O_4:Eu^{2+}$, Nd^{3+} and (D) commercial ZnS:Cu, Co. (Reprinted with permission from ref 11. Copyright 1996 Electrochemical Society.)

With respect to both initial intensity (y-axis in Figure 1) and the emission lifetime (x-axis in Figure 1), $SrAl_2O_4:Eu^{2+}$, Dy^{3+} outperformed its ZnS:Cu,Co predecessor, despite being non-radioactive. Essentially, Matsuzawa's phosphor addressed both of the most prominent obstacles for widespread ZnS:Cu commercialization—its toxicity and short-lived persistence—and brought a new realm of potential storage phosphors to light.

The discovery of $SrAl_2O_4:Eu^{2+}$, Dy^{3+} spawned a sudden upturn of scientific interest in the development of persistent-luminescent materials that could replace ZnS:Cu,Co; according to the Web of Science, over 87% of scientific journal articles on storage phosphors were published in the two decades following 1996, despite the prominence of ZnS:Cu,Co for over 100 years prior. Since 1996, over 200 storage phosphor systems have been developed—like $SrAl_2O_4:Eu^{2+}$, Dy^{3+}, most of these are comprised of an aluminate, gallate, silicate, or oxide host doped with one or more rare earth activating ions.[12] However, even with an increase in candidates, $SrAl_2O_4:Eu^{2+}$, Dy^{3+} remains an industry frontrunner due to its high quantum efficiency, tunable emission[13], chemical stability, non-radioactivity, bright initial luminescence[7], and long afterglow, reported to last up to 50 hours.[9,14]

Photoluminescence: Emission and Excitation

Materials that exhibit photoluminescence absorb energy in the form of photons, or light. Photons of sufficient energy are absorbed by the crystal lattice, dopants, or both, which causes an electron in the valence band to transition from the ground state to a higher-energy state. This process—promoting an electron from the ground state configuration to an excited state—is referred to as *excitation*. By definition, the excited state is not indefinitely

sustainable; the excited electron quickly relaxes back to the ground state, and the "excess" energy absorbed during excitation is released as a photon of a corresponding frequency/wavelength. The light released by the molecule is its *emission*, and the energies of the released photons indicate emission color. Thus, after excitation increases the net energy of a crystalline material, emission restores the lattice to its original configuration and releases the energy difference as photons. The emission has a lower frequency and longer wavelength than the corresponding excitation value due to nonradiative transitions—i.e., mechanisms of electron relaxation that do not produce a photon—in the molecule.[15]

Consider a phosphor with a fixed, stable crystal structure. Barring any extreme environmental conditions (e.g., change in temperature or pressure), the difference in energy between the highest occupied molecular orbital (HOMO) and the lowest unoccupied molecular orbital (LUMO) is fixed. Consequently, the amount of energy required to promote an electron from the HOMO to the LUMO and the amount of energy released as it reverts to the ground state are finite and constant. The energy released is proportional to the wavelength of the emission; thus, a stable, defined crystal matrix emits one or more wavelengths that are characteristic of that specific host/dopant structure.

In order to explain how Eu^{2+} and Dy^{3+} dopants affect the emission of strontium aluminate, it is necessary to consider how they are integrated into the host matrix. Strontium aluminates (SAO) can express five different defined phases, all of which are stable hosts: $SrAl_2O_4$, $SrAl_4O_7$, $SrAl_{12}O_{19}$, $Sr_3Al_2O_6$, and $Sr_4Al_{14}O_{25}$.[16] To form an SAO matrix, chains of AlO_x polyhedra create negatively charged cavities, and strontium cations are integrated into these cavities to restore charge neutrality.[13] Because divalent europium and strontium ions are similar in size—1.09 Å and 1.12 Å, respectively—Eu^{2+} integrates into Sr^{2+} sites in the

matrix whenever Sr^{2+} is stoichiometrically deficient.[17] In monoclinic $SrAl_2O_4:Eu^{2+},Dy^{3+}$, there are two crystallographically different Sr^{2+} sites that have the same coordination number and similar orientations within the matrix; therefore, Eu^{2+} ions have two potential sites to integrate into, resulting in a broad emission band.[18]

The $SrAl_2O_4:Eu^{2+}$, Dy^{3+} storage phosphor, like many other matrices doped with europium and dysprosium, is excited by ultraviolet light and emits visible light. Combined emission and excitation spectra of $SrAl_2O_4:Eu^{2+}$, Dy^{3+} are shown in Figure 2.

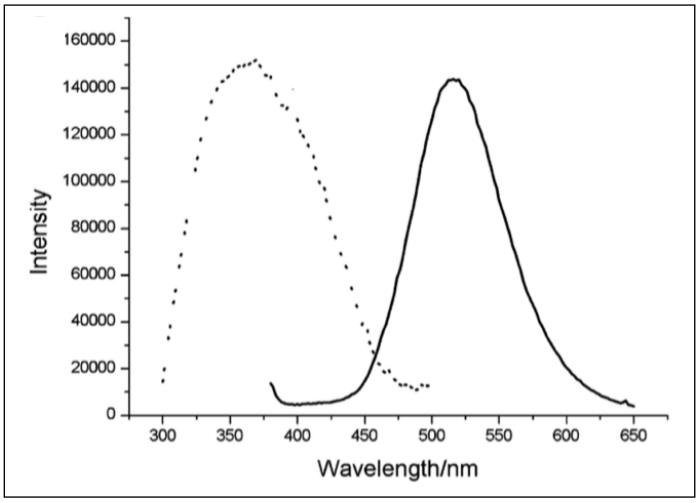

Figure 2. Excitation (dashed) and emission (solid) spectra of $SrAl_2O_4:Eu^{2+}$, Dy^{3+}. (Reprinted with permission from ref 19. Copyright 2007 Elsevier.)

The excitation peak, shown as a dashed line in Figure 2, stretches from ~300 nm to ~450 nm and is centered at 370 nm in the UV region. The broad excitation band allows for both indoor and outdoor use, as the material can be excited by both sunlight and indoor fluorescent light.

The strong emission peak in Figure 2 falls within the visible spectrum, stretching from 450 nm to 650 nm and centered at ~525 nm. The energy absorption, electron transition, and resulting emission are carried out by the divalent europium ion; i.e., Eu^{2+} is the

luminescence center of the $SrAl_2O_4:Eu^{2+}$, Dy^{3+} phosphor.[20] When $SrAl_2O_4:Eu^{2+}$, Dy^{3+} is optically excited by UV light, a Eu^{2+} valence electron transitions from the $4f^7$ ground state to the $4f^65d^1$ excited state. The subsequent relaxation of the excited electron to the ground state produces photons of ~525 nm—green on the visible spectrum. This excitation mechanism must be taken into consideration during synthesis if the europium precursor is trivalent, as in $Eu(NO_3)_3$; if Eu^{3+} is not properly reduced to Eu^{2+} during synthesis, the necessary transition cannot happen and the phosphor emits red light due to electron transitions in the 4*f* levels instead of green.[21]

Although many other host matrices doped with Eu^{2+} also emit green light, the green emission is not characteristic of Eu^{2+}. For example, $CaAl_2O_4:Eu^{2+}$ exhibits a blue emission (~448 nm), while another calcium-based phosphor, $CaS:Eu^{2+}$, emits red (~651 nm).[17] This shift in emission is due to the nature of the orbitals in the aforementioned $4f^7 \rightarrow 4f^65d^1$ electron transition. The 5*d* orbital, typically devoid of electrons, is not strongly attracted to the nucleus and is sensitive to changes in the crystal field environment as a result.[7] Consequently, a change in crystal structure can affect the energy gap between the HOMO and the LUMO and, by definition, the energy released by an electron as it falls from $4f^65d^1$ to $4f^7$. The 5*d* orbital is sensitive enough to the crystal field environment that different molar ratios of SrO and Al_2O_3 can produce phosphors with distinct emissions. For example, $Sr_4Al_{14}O_{25}$ and $SrAl_2O_4$ emit at 490 nm and 525 nm, respectively, due to changes in crystal field splitting of 5*d* orbitals and covalent interactions with oxygen anions.[22]

The intensity of the emission is dependent on many properties, such as grain size and surface morphology of the $SrAl_2O_4:Eu^{2+}$, Dy^{3+} particles, the molar ratio of dopant ions to host ions, and the extent of Eu^{3+} reduction to Eu^{2+} during synthesis. Greater $SrAl_2O_4:Eu^{2+}$,

Dy^{3+} emission intensity creates a wider variety of potential applications for the phosphor, due not only to the increased brightness but also the widening of the excitation band, which expands the range of light sources that will activate the phosphor emission.

Persistent Luminescence

Persistent luminescence is categorized into four subtypes according to the duration of the lasting emission: Very Short Persistent Phosphorescence (VSPP) lasts on the same order of magnitude as the excited state; Short Persistent Phosphorescence (SPP), detectable by the human eye, lasts for seconds; Persistent Phosphorescence (PP) lasts for minutes; and Long Persistent Phosphorescence (LPP) lasts for tens of minutes to hours.[20] For the $SrAl_2O_4:Eu^{2+}$, Dy^{3+} storage phosphor system, the role of Dy^{3+} is analogous to the role of the radioactive isotope(s) in ZnS:Cu,Co—that is, to extend the LPP emission lifetime of the phosphor. There are many theories for the mechanism of $SrAl_2O_4:Eu^{2+}$, Dy^{3+} long persistent luminescence, but it is generally accepted that Dy^{3+} creates energy traps, or "holes", that recombine with electrons before they relax to the ground state[11], allowing the liberation of energy (as photons) over time rather than immediately after absorbance.[21]

In $SrAl_2O_4:Eu^{2+}$, Dy^{3+}, the trivalent dysprosium ion (0.91 Å) substitutes into vacant Sr^{2+} sites alongside Eu^{2+}. However, Dy^{3+} is believed to act as an auxiliary activator rather than a luminescence center[6], meaning Dy^{3+} ions increase population in the conduction band by serving as extra trapping centers.[20] The long persistent luminescence of $SrAl_2O_4:Eu^{2+}$, Dy^{3+} is shown in Figure 3, which compares the afterglow lifetime of phosphors synthesized by combustion with different fuels.

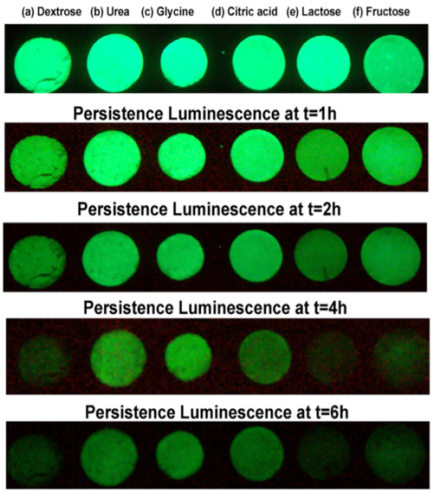

Figure 3. Afterglow luminescence of $SrAl_2O_4:Eu^{2+}$, Dy^{3+} synthesized by combustion route with different fuels. (Reprinted with permission from ref 18. Copyright 2015 Elsevier.)

Because the afterglow luminescence is dependent on the "depth" of the traps (and thus, the crystal structure), the synthesis route can have a significant effect on luminescence lifetime. This relationship is shown in Figure 3; the $SrAl_2O_4:Eu^{2+}$, Dy^{3+} phosphors synthesized with urea, glycine, and citric acid fuels exhibit brighter emissions for longer periods of time than those made with dextrose, lactose, and fructose fuels. Other synthesis parameters, such as the molar ratio of dysprosium to europium, can also extend or shorten the luminescence lifetime of $SrAl_2O_4:Eu^{2+}$, Dy^{3+}. A high Dy^{3+} content does not equate to a long afterglow; both Eu^{2+} and Dy^{3+} can "quench" the luminescence of the phosphor if the host to dopant ratio is sufficiently small.[9]

Synthesis Methods

It has been established that the color, emission intensity, and afterglow duration of the $SrAl_2O_4:Eu^{2+}$, Dy^{3+} storage phosphor are highly dependent on the crystal lattice. However, even sophisticated methods of microscopy and spectroscopy can fall short of detecting exact

changes to the matrix—such as difference in bond lengths or group orientation—that arise as the result of a new synthesis parameter or method. Fortunately, changing the crystal structure alters more readily observable properties of the particle, such as its size and surface morphology. Consequently, the bulk of scientific studies on the optical properties of $SrAl_2O_4:Eu^{2+}$, Dy^{3+} focus on developing synthesis methods that reliably produce particles with specific physical properties. Differences in emission intensity, peak wavelength, and afterglow are measured in relation to these observable changes; these relationships are used to confirm or deny hypotheses about changes in crystal structure.

As a result, an ideal synthesis method would offer a great degree of control over certain variables—particularly particle shape, size, surface morphology, and phase purity—so that specific properties of the phosphor can be altered to perform different studies or suit different applications. Furthermore, any practical method of synthesis should be relatively affordable, safe, and scalable for industrial purposes. Many different techniques emerged for the synthesis of persistent luminescent $SrAl_2O_4:Eu^{2+}$, Dy^{3+} phosphors after the initial discovery in 1996, including the sol-gel method, chemical precipitation method, hydrothermal co-precipitation method[1], laser synthesis[5], and flame-spray pyrolysis. However, these techniques leave much to be desired, and altering the synthesis method to improve one trait of the phosphor often results in the partial loss of another.

The simplest and most popular synthesis method is the solid state reaction technique (SSRT). SSRT involves grinding stoichiometric amounts of carbonate and oxide powders into a mixture that is sintered two to four times in a reductive atmosphere. Although the precursor materials for SSRT are relatively inexpensive, the heating process can take days to complete and requires reaction temperatures from 1200°C to 1600°C. Solid state reactions at

high temperatures produce microcrystalline products that vary in shape and tend to agglomerate.[9] This agglomeration and subsequent cooling causes the phosphor material to form a hard, dense mass that must be ground into a fine powder, introducing surface defects that reduce the efficiency of both dopant sites.[9,14] Many practical applications of persistent phosphors, such as LED surfaces and printing inks, require fine particles with a consistent size and shape[5]—properties that cannot be attained through SSRT alone.[23] Nevertheless, SSRT is a popular industrial synthesis method due to its affordability and ease of scalability, despite the long reaction time and post-treatments required to make particles suitable for application.[23]

Another prominent synthesis technique for $SrAl_2O_4:Eu^{2+}$, Dy^{3+} phosphor material is the combustion synthesis technique (CST). CST is a wet synthesis method, meaning that the solid metal nitrate precursors are mixed stoichiometrically into a solution with an organic fuel. The solution is heated at relatively low temperatures (500°C - 700°C); as it becomes more concentrated, an exothermic redox reaction takes place between the fuels and the metal nitrates.[23] This exothermic reaction produces a flame hot enough to complete synthesis, and the gases released during the reaction foster a reductive atmosphere sufficient for the Eu^{3+} to Eu^{2+} transition. The complete combustion reaction, from the time the solution is placed into the furnace to when it is removed as a final product, typically lasts five to fifteen minutes.[23] CST produces a light, fluffy solid that can be made into a fine powder without vigorous grinding, minimizing the introduction of surface defects and better preserving the emission intensity of the phosphor. Furthermore, because dissolving the precursors into a solution ensures a greater degree of homogeneity than grinding solids into a uniform mixture, phosphors synthesized by CST are typically of higher phase purity than those made by

SSRT.[14] However, despite its many benefits, CST is more difficult to adapt to an industrial environment due to the exothermic nature of the reaction.

CST differs from SSRT in that it requires a fuel to facilitate synthesis—the fuel is responsible for the fast reaction time. Commonly used organic fuels include urea (CH_4N_2O) and glycine ($C_2H_5NO_2$), as is shown in Figure 3. The role of the fuel in combustion synthesis is to facilitate an oxidation-reduction reaction with the metal nitrates (oxidizers) in solution.[23] The ignition of the redox reaction at 500°C produces a flame that raises the reaction temperature enough to produce the desired crystal phase, as 500°C alone is not sufficient. Furthermore, the reductive reaction atmosphere that converts Eu^{2+} to Eu^{3+} is a direct result of escaping gases caused by fuel ignition. The SSRT process involves heating the material to adequately high reaction temperatures within a furnace, and the reductive atmosphere is provided externally rather than a product of the reaction itself. Thus, a fuel is not necessary for SSRT.

SSRT and CST are similar in that incorporating a flux material, such as boric acid, can assist in improving the emission intensity and afterglow duration of the storage phosphor.[23] At high concentrations, boric acid facilitates the substitution of B^{3+} into Al^{3+} sites in the Al_2O_3 polyhedra. This forms aluminoborate matrix phases that distort the crystallographic structure of the phosphor, changing its emission in both intensity and wavelength.[25] However, even at concentrations as low as 1% mol, the addition of boric acid during synthesis lowers the reaction temperature for $SrAl_2O_4$:Eu^{2+}, Dy^{3+} as well as other storage phosphor systems. For example, Haranath *et al*. determined that a boric acid flux can lower the reaction threshold between $CaAl_2O_4$: Eu^{2+}, Dy^{3+} precursors by 60°C.[26] Lowering the required reaction temperature reduces the amount of energy needed to carry out the

reaction, ensuring that all of the precursor materials react and do not leave unreacted oxide, nitrate, or carbonate impurities in the phosphor product. Furthermore, the flux facilitates the integration of the activator ion (Eu^{2+}) into the matrix, increasing the density of the luminescence centers in the matrix and, as a result, the emission intensity.[26] This increase in initial luminescence intensity, as well as the improved formation of traps due to better integration of the auxiliary activator (Dy^{3+}) lengthens the afterglow lifetime.[24]

For the synthesis of strontium aluminate phosphors, CST and SSRT share several benefits over less common synthesis methods. The precursor materials for CST and SSRT are relatively affordable, non-toxic, and easy to store. Both processes can be carried out safely without a formal chemistry education, and the required equipment is standard in synthesis industries and laboratories. Aside from energy consumption, neither method poses a significant threat to the environment. Although the synthesis parameters differ, CST and SSRT can produce storage phosphors that exhibit equal photoluminescence intensity, as is shown by Son *et al.* in Figure 4.

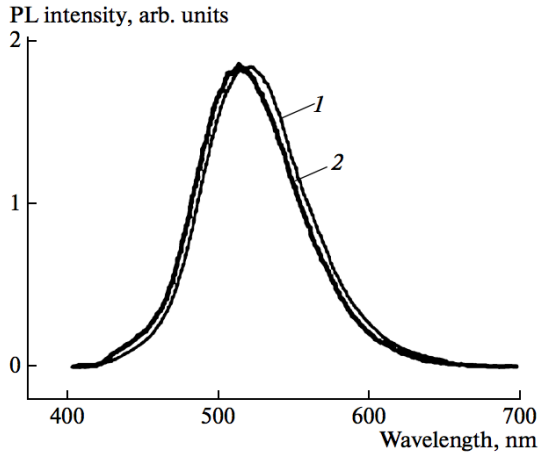

Figure 4. Photoluminescence spectra of $SrAl_2O_4:Eu^{2+}$, Dy^{3+} prepared by (1) the solid-state method and (2) the combustion technique. Figure by Son *et al.* is licensed under CC BY-NC-ND 3.0 (Reprinted from ref 27.)

In Figure 4, both SSRT and CST produce photoluminescence peaks of equal width and height, the only difference being a slight blue shift in the SSRT spectrum. This is likely due to minute differences in the matrices produced by both techniques. The most important benefit of both methods is that they offer straightforward, simple techniques to manipulate specific properties of the phosphor product, allowing for reliable reproduction of phosphors with desired matrix structures.

However, when comparing CST and SSRT, the former exhibits several benefits over the latter. CST is much faster; the reaction is complete within mere minutes rather than over the course of 2-3 days. Because CST reactions are self-propagating, each reaction only requires temperatures from 500°C to 700°C for a brief period of time. This consumes far less energy than SSRT, which requires 2-3 heating cycles from 1200°C to 1600°C for 20+ hours. Furthermore, the exothermic CST reaction creates its own reductive atmosphere, whereas the reductive atmosphere must be supplied during the SSRT heating process. For CST experiments, inexpensive mainstream equipment can be used, making CST a more feasible approach for industry adaptation versus SSRT. The combustion precursor solution offers greater assurance of homogeneity than a mixture of solids; coupled with the short reaction time and significant decrease in required grinding, this results in finer particles with higher phase purity and fewer surface defects.[14]

CST typically produces smaller particles than SSRT due to the escape of gases during the reaction, and it offers more flexibility in tuning the particle size—CST can reliably produce nanoparticles under certain reaction conditions[7,9,18], whereas SSRT nanoparticle synthesis requires extensive grinding that decreases the emission intensity of the phosphor.[9] Compared to bulk samples, nano-phosphors are often preferable for practical applications

due to their high packing density, low light-scattering effects, and easy suspension in liquid media.[23] Although SSRT is more easily scalable than CST, the benefits of CST far outweigh its disadvantages for the widespread development of storage phosphor applications.

Characterization

Spectrofluorometry is a popular characterization method for collecting and analyzing the excitation and emission spectra of photoluminescent materials. Spectrofluorometry is particularly useful for comparing differences in emission intensity and/or wavelength within a given series, allowing researchers to quickly form a hypothesis regarding the effect of a given parameter on the crystal matrix and pursue subsequent characterization methods to confirm or deny this hypothesis. Figure 5 is an example of an emission graph generated by spectrofluorometry.

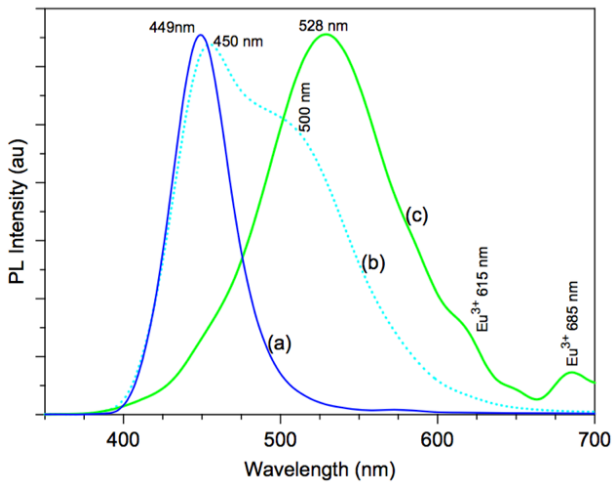

Figure 5. Emission spectra of (a) $CaAl_2O_4:Eu^{2+}$, Dy^{3+}, (b) $BaAl_2O_4:Eu^{2+}$, Dy^{3+}, and (c) $SrAl_2O_4:Eu^{2+}$, Dy^{3+}. (Reprinted with permission from ref 28. Copyright 2009 Elsevier.)

Figure 5 compares the emission spectra of three storage phosphor hosts, $CaAl_2O_4$, $BaAl_2O_4$, and $SrAl_2O_4$, doped with Eu^{2+} and Dy^{3+}. Emission spectra depict the intensity of the phosphor emission (y-axis) at each wavelength within a given range (x-axis) under a fixed excitation wavelength (λ_{ex}). The emission wavelength that exhibits the greatest intensity for a storage phosphor material is its peak emission (λ_{em}). If this peak falls within the visible range, λ_{em} is indicative of the color of the emission to the human eye. As is shown in Figure 5, $CaAl_2O_4$:Eu^{2+}, Dy^{3+} emits at 449 nm; $BaAl_2O_4$:Eu^{2+}, Dy^{3+} emits at 450 nm and 500 nm; and $SrAl_2O_4$:Eu^{2+}, Dy^{3+} emits at 528 nm, 615 nm, and 685 nm, respectively.[28] This suggests that substituting different Group 3 metal ions into the Al_2O_3 polyhedra results in contraction or expansion of the bonds in the crystal matrix, causing shifts in emission wavelength. Furthermore, the emission peaks at 615 nm and 685 nm for $SrAl_2O_4$:Eu^{2+}, Dy^{3+} indicate that the reported synthesis method did not fully convert Eu^{3+} to Eu^{2+}, because a red emission in this system is caused by the presence of Eu^{3+}.[21] The relative intensities of the small red peaks compared to the 528 nm peak (due to Eu^{2+}) signify that, in relation to Eu^{2+} ions, there are few Eu^{3+} ions dispersed in the matrix, and the chosen synthesis method could potentially achieve full conversion with more fuel.

Emission spectra are acquired by measuring the emission intensity at varying wavelengths using a fixed excitation wavelength. Conversely, excitation spectra are obtained using a specific λ_{em}, and a range of excitation wavelengths is collected. An example of this is shown in Figure 6, which compares the excitation spectra of $SrAl_xO_y$:Eu^{2+}, Dy^{3+} storage phosphors with varying Eu^{2+}:Dy^{3+} ratios.

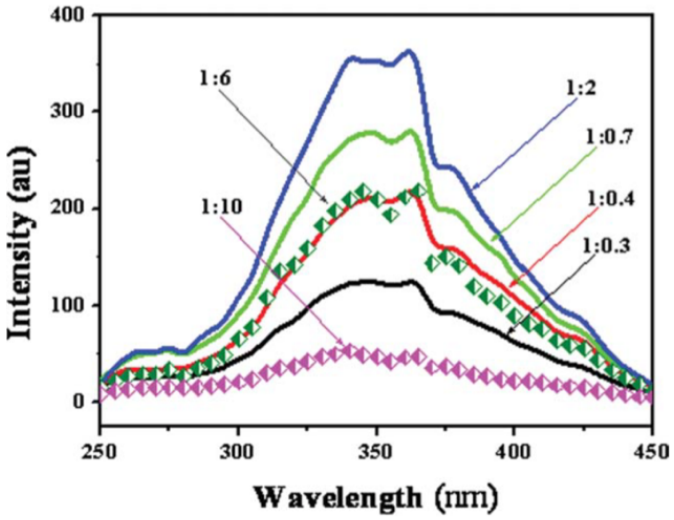

Figure 6. Excitation spectra of $SrAl_xO_y:Eu^{2+}$, Dy^{3+} with Eu^{2+}:Dy^{3+} molar ratios from 1:0.3 to 1:10 (λ_{em} = 515 nm). (Reprinted with permission from ref 13. Copyright 2010 John Wiley and Sons.)

As is shown in Figure 6, the optimal excitation wavelength for the 515 nm emission of $SrAl_xO_y:Eu^{2+}$, Dy^{3+} phosphors produced by Bem *et al.* is ~365 nm, and the entire peak stretches from approximately 300 to 400 nm.[13] Figure 6 also shows that changing the molar ratios of Eu^{2+} to Dy^{3+} from 1:0.3 to 1:10 produces significant changes in the intensity of λ_{em}. As Dy^{3+} increases from 1:0.3 to 1:2, the 515 nm emission intensity steadily increases. As Dy^{3+} is increased further (1:6 and 1:10), the emission intensity decreases sharply, indicating that the sample has been quenched by the Dy^{3+} content. This relationship is mirrored in the corresponding emission spectra, shown in Figure 7.

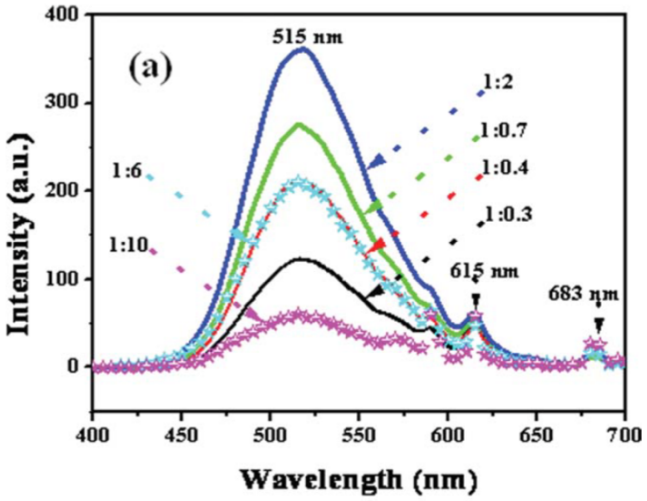

Figure 7. Emission spectra of $SrAl_xO_y:Eu^{2+}$, Dy^{3+} with Eu^{2+}:Dy^{3+} molar ratios from 1:0.3 to 1:10. (Reprinted with permission from ref 13. Copyright 2010 John Wiley and Sons.)

These emission spectra, like the excitation spectra in Figure 6, indicate that 1:2 is the ideal Eu^{2+}:Dy^{3+} ratio for the 515 nm emission of this phosphor system. Emission and excitation spectra are often combined into a single graph (Figure 2 is an example of this).

Emission and excitation spectra of photoluminescent phosphor materials are collected using a spectrofluorometer, or fluorometer. A diagram of a standard fluorometer is shown in Figure 8.

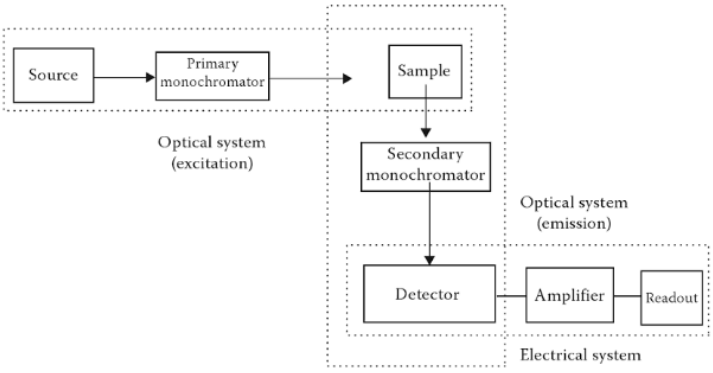

Figure 8. Block diagram of a standard fluorometer. (Reprinted with permission from ref 2. Copyright 2014 Taylor & Francis Group.)

To produce a spectrum, the excitation radiation is generated by a light source (indicated by "Source" in Figure 8). Xenon arc lamps are commonly found as fluorometer light sources due to their intense emission from 200 nm into the infrared (IR).[2] Before reaching the sample chamber, the excitation source passes through the primary monochromator—a wavelength selection device—which filters the broad spectrum source into a narrow band of desired wavelengths to be absorbed by the sample.[2] The sample emits under excitation, and the emission passes through a secondary monochromator that specifies the wavelength measured by the detector and "filters" out background signal from the excitation source. The detector measures the signal from the phosphor emission. Ideally, a fluorometer would be sealed completely from external light, the white light source would exhibit a consistent intensity over time, and the detector would read all wavelengths with equal sensitivity. However, this is almost never the case, and the intensity read by the emission detector is subjected to a series of correction functions to account for these inconsistencies (as well as the dark current inherent in the detector) before producing excitation or emission spectra.

A fluorometer can also be used to collect luminescence decay curves to determine the length of persistent luminescence. Unlike emission and excitation spectra, decay curves measure a single wavelength of the phosphor emission after excitation by a single wavelength. Therefore, the intensity of the emission (y-axis) is plotted in relation to time (x-axis) rather than over a range of wavelengths. In order to produce a decay curve, the sample is exposed to a specific excitation wavelength for a given period of time. Once the excitation source is removed, the fluorometer measures the intensity of the phosphor emission at a fixed wavelength over time. The resulting exponential decay curve can be modeled using a second-or-third-order differential equation that relates intensity to time. If the persistent emission

outlasts the collection period, this equation can be used to estimate the amount of time the phosphor emits; it can also be used to determine the amount of time the phosphor emits at an intensity above a given threshold.

While the emission and excitation spectra can shed light on the electronic properties of a phosphor, they are not as useful for identifying structural properties, such as phases and impurities present within the material. Impurities and mixed phases are good indicators of the success or failure of a synthesis method, as their presence in a sample can cause the luminescence output to diminish. X-ray powder diffraction (XRD) is a much more informative method of analyzing these structural properties. XRD involves the bombardment of the phosphor sample by monochromatic X-rays. The constructive and destructive interference of the beams reflected from the atomic planes in the crystal form a diffraction pattern.[2] This pattern is typically referenced to a database of standard diffraction patterns for known crystalline materials. An example of an XRD spectrum is shown in Figure 9.

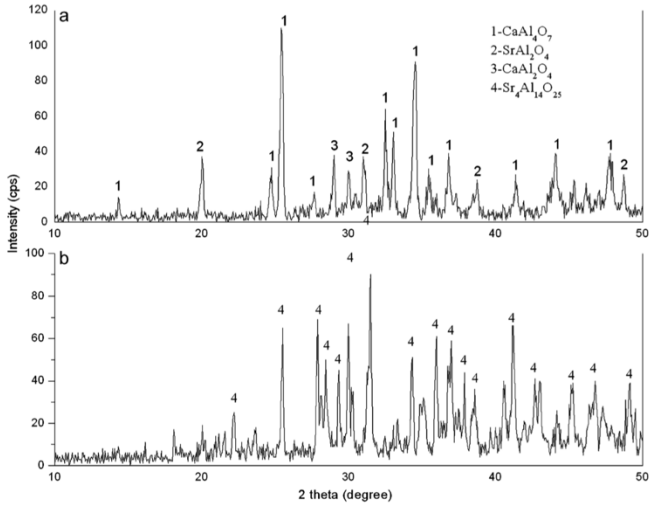

Figure 9. XRD spectra of (a) $Sr_{0.8}Ca_{3.2}Al_{14}O_{25}:Eu^{2+}$, Dy^{3+} and (b) $Sr_4Al_{14}O_{25}:Eu^{2+}$, Dy^{3+}. (Reprinted with permission from ref 29. Copyright 2008 Elsevier.)

Figure 9 compares the phase compositions of $Sr_4Al_{14}O_{25}:Eu^{2+}$, Dy^{3+} with and without Ca^{2+} substitution for Sr^{2+}.[29] A diffraction pattern consists of a series of peaks used to identify the compounds present in a material. The signal intensity (typically counts per second) is mapped as a function of the diffraction angle of the reflected beams. As is shown in Figure 9, without Ca^{2+} substitution, $Sr_4Al_{14}O_{25}:Eu^{2+}$, Dy^{3+} was synthesized in the pure, desired phase, indicated by the "4 – $Sr_4Al_{14}O_{25}$" assigned to every peak. However, with Ca^{2+} substitution by 80 mol%, three additional aluminate phases were produced ($CaAl_4O_7$, $SrAl_2O_4$, and $CaAl_2O_4$), which indicates that the Ca^{2+} ion disrupts the formation of the $Sr_4Al_{14}O_{25}:Eu^{2+}$, Dy^{3+} phosphor matrix.

XRD can be used to estimate the percent composition of the compounds in the material, including those of different phases (e.g., $SrAl_2O_4$, $SrAl_4O_7$, $SrAl_{12}O_{19}$, etc.). Ideally, the produced phosphor will consist entirely of the desired phase without any intermediate or precursor compounds, as is shown in Figure 9b above. The presence of alternate phases of the phosphor can result in a non-uniform emission[16] and detract from the quality of the material. XRD is a useful resource for determining how the synthesis parameters should be altered. The presence of extraneous phases and/or compounds in the diffraction pattern often points to a specific synthesis parameter. For example, if the XRD pattern shows a precursor compound is present, this compound would be reduced in future experiments to favor 100% conversion to the desired phase.

As was discussed earlier, the surface composition, particle size, and degree of agglomeration of storage phosphor particles can be affected by a change in composition or altered synthesis method. While XRD can provide extensive information on the crystal structure of the material, it does not produce meaningful data regarding the surface

morphology of the storage phosphor; thus, XRD alone is not sufficient for evaluating all structural properties of the matrix. Therefore, the storage phosphor particles will also be imaged using scanning-electron microscopy (SEM), which has the potential to map the shape of the particles to the nanometer range. SEM images are extremely useful for determining how certain synthesis parameters alter the surface morphology and particle size of a storage phosphor. A series of SEM images are shown in Figure 10.

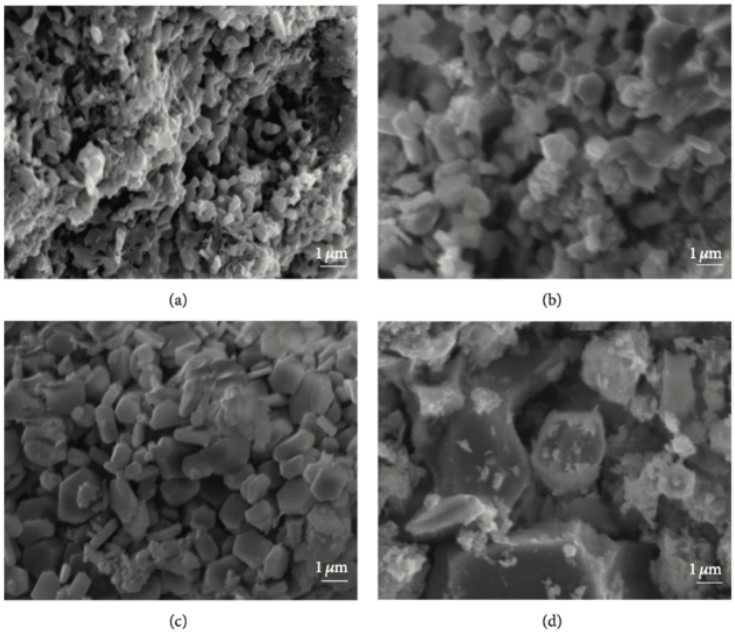

Figure 10. SEM images of $Sr_4Al_{14}O_{25}:Eu^{2+}$, Dy^{3+} phosphors prepared with H_3BO_3 flux concentrations of (a) 0 mol%, (b) 20 mol%, (c) 40 mol%, and (d) 100 mol%. Figure by Luitel *et al.* is licensed under CC BY 3.0 (Reprinted from ref 30.)

Figure 10 compares a series of $Sr_4Al_{14}O_{25}:Eu^{2+}$, Dy^{3+} storage phosphors synthesized with different molar concentrations of boric acid flux. The scale bar at the bottom right of each picture indicates the relative size of the particles. In Figure 10, SEM shows that the particles grow from sub-micron size to several tens of micrometers large as the boric acid concentration is increased. This suggests that the boric acid flux increases the degree of

melting and agglomeration during synthesis, which could be undesirable for applications that require nanoparticle phosphors, such as printing.[5]

Spectrofluorometry, XRD, and SEM are not the only methods of storage phosphor characterization. However, emission and excitation spectra, luminescence decay models, phase composition, and particle size, shape and surface morphology provide sufficient insight into the storage phosphor matrix to draw conclusions about the success of the synthesis method, the optical efficiency of the phosphor material, and its viability for use in practical applications.

$SrAl_2O_4:Eu^{2+}$, Dy^{3+} has been a popular storage phosphor in scientific research and industry since its discovery in 1996. It has been shown that the optical properties of this storage phosphor are sensitive to changes in the crystal matrix, and that substituting ions into the host matrix can significantly change the color of the emission. The aim of this project is to synthesize an SAO-based, Ca^{2+}-substituted storage phosphor ($Sr_{1-x}Ca_xAl_2O_4:Eu^{2+}$, Dy^{3+}) that is more efficient than non-substituted $SrAl_2O_4:Eu^{2+}$, Dy^{3+} for the eventual purpose of developing a printing ink with SAO nanomaterials.

CHAPTER II

MATERIALS AND METHODS:
PHOSPHOR SYNTHESIS AND ANALYSIS

Various series of storage phosphors were produced using a small-scale combustion synthesis technique. CST was chosen for this project due to its short reaction time, high emission intensity, low reaction temperature, and high degree of precursor homogeneity.

Materials

The following metal nitrates were used for combustion synthesis of $Sr_{1-x}Ca_xAl_2O_4:Eu^{2+}$, Dy^{3+} storage phosphors: $Sr(NO_3)_2$ [CAS #10042-76-9, Sigma-Aldrich Lot MKBW7822V, ≥99.0%], $Ca(NO_3)_3{\cdot}4H_2O$ [CAS #13477-34-4, Alfa-Aesar Lot 23368, 99.98%], $Al(NO_3)_3{\cdot}9H_2O$ [CAS #7784-27-2, Alfa-Aesar Lot N03C026, 98%], $Eu(NO_3)_3{\cdot}6H_2O$ [CAS #10031-53-5, Alfa-Aesar Lot Q20C039, 99.9%], and $Dy(NO_3)_3{\cdot}5H_2O$ [CAS #10031-49-9, Alfa-Aesar Lot 22475, 99.99%]. Boric acid (H_3BO_3) [CAS #10043-35-3, Sigma-Aldrich Lot 112K0971, ≥99.5%] was incorporated as a flux, and urea (CH_4N_2O) [CAS #57-13-6] was used as a fuel. Distilled, deionized water was obtained from a Barnstead Nanopure Diamond distillation apparatus (17.8 MΩ-cm) with a filter attachment (0.2 μm pore size, Lot 109-1099B).

Phosphor Synthesis

For each respective series of samples, all parameters within the phosphor matrix were held constant except that being optimized. For example, the first parameter optimized for the $Sr_{1-x}Ca_xAl_2O_4:Eu^{2+}$, Dy^{3+} phosphor system was the ratio of Sr^{2+} to Ca^{2+} in the matrix; thus, a series of $Sr_{1-x}Ca_xAl_2O_4$: 3 mol% Eu^{2+}, 1 mol% Dy^{3+} phosphors were synthesized with varying Sr^{2+}:Ca^{2+} ratios from 1:0 to 0:1 (x = 0, 0.1, 0.3, 0.5, 0.7, 0.9, 1.0). The sample that exhibited the best performance in each series was selected for further optimization. The parameters chosen for the optimization of $Sr_{1-x}Ca_xAl_2O_4:Eu^{2+}$, Dy^{3+} are shown in Table 1.

Table 1. Synthesis parameters for storage phosphor optimization

Series ID	Parameter	General Formula	Samples
S1	Sr^{2+}:Ca^{2+}	$Sr_{1-x}Ca_xAl_2O_4$: 3 mol% Eu^{2+}, 1 mol% Dy^{3+}	x = 0, 0.1, 0.3, 0.5, 0.7, 0.9, 1.0
S2	Eu^{2+} mol%	$Sr_{0.9}Ca_{0.1}Al_2O_4$: x mol% Eu^{2+}, 1 mol% Dy^{3+}	x = 1, 3, 5, 6, 7
S3	Dy^{3+} mol%	$Sr_{0.9}Ca_{0.1}Al_2O_4$: 6 mol% Eu^{2+}, x mol% Dy^{3+}	x = 1, 3, 5, 7
S4	Eu^{2+}:Dy^{3+}	$Sr_{0.9}Ca_{0.1}Al_2O_4$: (7 - x) mol% Eu^{2+}, x mol% Dy^{3+}	x = 1, 2, 3, 4, 6
S5	H_3BO_3 mol%	$Sr_{0.9}Ca_{0.1}Al_2O_4$: 6 mol% Eu^{2+}, 1 mol% Dy^{3+}, x mol% H_3BO_3	x = 10, 15, 20, 30, 40

The parameters were not varied uniformly across each series, as is evident in Table 1. For example, although a sample with 6 mol% Eu^{2+} was synthesized in S2, a 6 mol% Dy^{3+} sample was not synthesized in S3. This discrepancy arises with the emergence of clear trends early in data collection. In S3, the phosphor emission steadily decreased as Dy^{3+} content increased from 1 mol%, so a 6 mol% Dy^{3+} sample was not necessary to conclude that the optimum Dy^{3+} content was 1 mol% for the given phosphor system. Conversely, emission intensity

increased as Eu^{2+} content increased up to 5 mol% before decreasing sharply at 7 mol%; thus, a 6 mol% Eu^{2+} sample was synthesized to determine if the emission intensity continued to increase after 5 mol% or if 5 mol% was the ideal Eu^{2+} concentration in the matrix for the chosen synthesis method.

In order to carry out the combustion reactions for the five series listed in Table 1, stoichiometric amounts (1/85 molar scale) of the metal nitrates, H_3BO_3, and urea were measured using a Mettler-Toledo XS105 DualRange analytical balance (±0.01 mg). These solid materials were then added with a stir bar to 40 mL of water in a 600 mL beaker. Urea was chosen as a fuel because it fosters a reductive atmosphere, causes a facile reaction, and produces enough energy in the oxidation-reduction reaction to complete synthesis at 500 °C due to its high exothermicity.[13] In order to ensure facilitation and completion of the reaction[31], urea was added to the precursor solution at 3x stoichiometric excess (11.75 mol eq.). The precursor solution was stirred at 60 °C for approximately 10 minutes to allow complete dissolution and ensure homogeneity.

A Sentro Tech ST-1600-101012 high-temperature box furnace was ramped to 500 °C prior to the combustion reaction. For rapid combustion, it is important that the solution is only exposed to the target temperature rather than a gradual ramp process; otherwise, combustion could take place at a lower temperature, which would provide insufficient energy to form the desired product. The beaker containing the precursor solution was placed directly into the 500 °C furnace. The entire combustion process—i.e., concentration of the solution, ignition, and crystal formation—lasted 13 minutes, producing a yellow-green, fluffy phosphor material. The beaker was removed immediately after the reaction was complete in order to avoid further changes of the crystal matrix, which could result in reduced emission

intensity, a shift in peak emission wavelength, or both. Furthermore, immediate removal of the beaker also prevents the oxidation of Eu^{2+} to Eu^{3+} after the reductive atmosphere dissipates.

The combustion product was lightly ground in an agate mortar for 5 minutes to produce a fine, homogeneous powder. Excessive grinding, which is required for many phosphor synthesis techniques (most notably SSRT), generates surface defects that can affect the $4f^7 \rightarrow 4f^6 5d^1$ bandgap and/or serve as alternate sites for photon absorption, lowering the emission intensity and efficiency of the phosphor product.

Analysis and Characterization

In order to examine the visible differences in emission and afterglow time among phosphors in each series, the materials were imaged under 365 nm excitation and at intervals 5 s and 10 s after excitation using an 8-megapixel camera with a 29 mm focal length and f/2.2 aperture.

Emission, excitation, and luminescence decay spectra were collected on a Horiba Fluorolog FL3-12 spectrofluorometer. A 450 W xenon arc lamp was used as the source for the fluorometer. Prior to each collection, an excitation spectrum (λ_{em} = 350 nm) was collected of the empty sample chamber in order to calibrate the lamp, and an emission spectrum (λ_{ex} = 365 nm) was collected of a deionized water sample for detector calibration. The primary grating had 1200 mm grooves and a blaze wavelength of 330 nm, and the secondary grating had 1200 mm grooves and a blaze wavelength of 500 nm. Emission and excitation spectra were collected with primary and secondary slit widths of 0.85 nm.

Luminescence decay spectra were collected at λ_{em} = 525 nm after excitation of the sample (λ_{ex} = 365 nm) for 1 minute; the primary and secondary slit widths were 3.25 nm.

To perform structural analysis and determine phase purity of $Sr_{1-x}Ca_xAl_2O_4:Eu^{2+}$, Dy^{3+} samples, x-ray diffraction patterns were collected at room temperature with a PANalytical Empyrean diffractometer under Cu-Kα radiation. The 2θ scan range was 5 – 90 at increments of 0.02626, and the current was 40 kV. Further physical characterization by SEM imaging was carried out on a Hitachi S-4700 Field Emission Scanning Electron Microscope with a 1.5 kV potential and 20 microamp current.

CHAPTER III

RESULTS AND DISCUSSION

Due to its bright emission, long persistent luminescence lifetime, and chemical stability, the $SrAl_2O_4:Eu^{2+}$, Dy^{3+} storage phosphor system was chosen to be optimized for the development of a colloidal nanoparticle ink solution. It has been shown that the substitution of other Group 3 alkaline earth metals into strontium aluminate matrices can increase the luminescence intensity of the phosphor.[32,33] For this project, Ca^{2+} was chosen as the substitute metal ion in the $SrAl_2O_4:Eu^{2+}$, Dy^{3+} matrix.

Optimization of S1 Phosphor Series: $Sr_{1-x}Ca_xAl_2O_4$: 3 mol Eu^{2+}, 1 mol% Dy^{3+}

The first optimization parameter for Ca^{2+}-substituted $SrAl_2O_4:Eu^{2+}$, Dy^{3+} storage phosphors was the extent of Sr^{2+} substitution by Ca^{2+} in the host matrix. To examine the effect of strontium ion substitution on λ_{em} and the emission intensity of the phosphor, a series of $Sr_{1-x}Ca_xAl_2O_4:Eu^{2+}$, Dy^{3+} phosphors (S1), where $x = 0$, 0.1, 0.3, 0.5, 0.7, 0.9, and 1.0, were synthesized by combustion route. Europium(II) and dysprosium(III) content were fixed at relatively low values (3 mol% and 1 mol%, respectively) to avoid quenching of the phosphor material. To confirm that the S1 phosphors were synthesized in the correct phase and to analyze changes in crystal structure with the addition of Ca^{2+} content, XRD spectra were

collected for $SrAl_2O_4:Eu^{2+}$, Dy^{3+}; $Sr_{0.7}Ca_{0.3}Al_2O_4:Eu^{2+}$, Dy^{3+}; $Sr_{0.5}Ca_{0.5}Al_2O_4:Eu^{2+}$, Dy^{3+}; $Sr_{0.3}Ca_{0.7}Al_2O_4:Eu^{2+}$, Dy^{3+} and $CaAl_2O_4:Eu^{2+}$, Dy^{3+}. XRD results are shown in Figure 11.

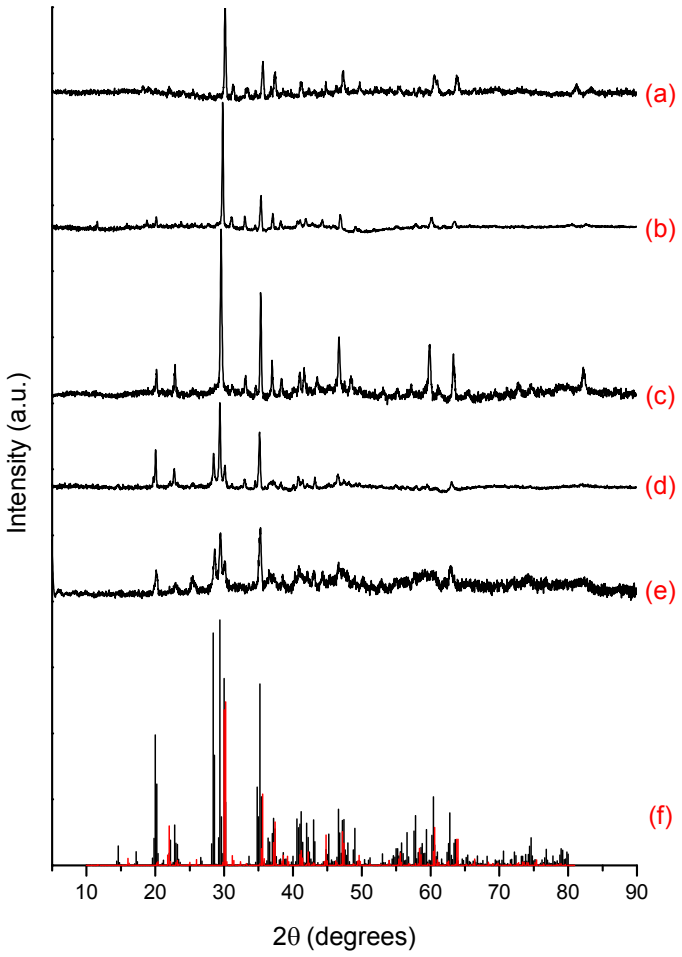

Figure 11. XRD spectra for S1 phosphors: (a) $CaAl_2O_4$: 3 mol% Eu^{2+}, 1 mol% Dy^{3+}, (b) $Sr_{0.3}Ca_{0.7}Al_2O_4$: 3 mol% Eu^{2+}, 1 mol% Dy^{3+}, (c) $Sr_{0.5}Ca_{0.5}Al_2O_4$: 3 mol% Eu^{2+}, 1 mol% Dy^{3+}, (d) $Sr_{0.7}Ca_{0.3}Al_2O_4$: 3 mol% Eu^{2+}, 1 mol% Dy^{3+}, (e) $SrAl_2O_4$: 3 mol% Eu^{2+}, 1 mol% Dy^{3+}, and (f) reference spectra for $SrAl_2O_4$ (black, ICSD no. 291361) and $CaAl_2O_4$ (red, ICSD no. 157457)

Characteristic $CaAl_2O_4$ peaks appeared at 30.187°, 35.656°, 37.509°, 60.623°, and 64.041° in the $CaAl_2O_4$ reference spectrum (Figure 11f, shown in red). These peaks were also present in the experimental $CaAl_2O_4$: 3 mol% Eu^{2+}, 1 mol% Dy^{3+} spectrum (Figure 11a). For

$SrAl_2O_4$, characteristic peaks appeared at 20.196°, 22.843°, 28.466°, 29.393°, and 30.032° in the reference spectrum (Figure 11f, shown in black). These peaks were also present in the experimental $SrAl_2O_4$: 3 mol% Eu^{2+}, 1% Dy^{3+} spectrum (Figure 11e). No precursor peaks were apparent in Figures 11a or 11e, suggesting that both products were homogeneous. Thus, combustion with the given parameters was determined to be a suitable method for synthesizing S1 phosphors, $Sr_{1-x}Ca_xAl_2O_4$: 3 mol% Eu^{2+}, 1 mol% Dy^{3+}.

The XRD spectrum for the S1 phosphor with $x = 0.3$, $Sr_{0.7}Ca_{0.3}Al_2O_4$: 3 mol% Eu^{2+}, 1 mol% Dy^{3+}, is shown in Figure 11d. As Ca^{2+} content was raised from $x = 0$ to $x = 0.3$, the spectrum remained largely unchanged. All characteristic $SrAl_2O_4$ peaks that appeared in the reference and $x = 0$ spectra were also present in the $x = 0.3$ spectrum. Thus, when the sample composition was $Sr_{0.7}Ca_{0.3}Al_2O_4$: 3 mol% Eu^{2+}, 1 mol% Dy^{3+}, monoclinic $SrAl_2O_4$ was synthesized as the major phase, and Ca^{2+} ions were substituted into vacant Sr^{2+} sites in the matrix.

However, when the Ca^{2+} content was raised to $x = 0.5$, as is shown in Figure 11c, the XRD data resembled the $CaAl_2O_4$ reference spectrum rather than the $SrAl_2O_4$ reference spectrum. This change was indicated by the peaks that appeared at 29.724°, 35.171°, 36.892°, 59.983°, and 63.424°. It is important to note that these values were left-shifted by 0.560° on average compared to the $CaAl_2O_4$ reference. The $CaAl_2O_4$ phase forms at a lower temperature than the $SrAl_2O_4$ phase, so it is possible that $CaAl_2O_4$ was formed as the major phase with most of the Sr^{2+} ions incorporated into vacant Ca^{2+} sites. In addition to the $CaAl_2O_4$ peaks, Figure 11c also exhibited two characteristic $SrAl_2O_4$ peaks at 20.196° and 22.843°, which were not shifted compared to the $SrAl_2O_4$ reference. Liu *et al.* proposed that the Sr^{2+} ions not incorporated into $CaAl_2O_4$ react with Al^{3+} to form $SrAl_2O_4$ as a minor phase.

Thus, for $Sr_{0.5}Ca_{0.5}Al_2O_4$: 3 mol% Eu^{2+}, 1 mol% Dy^{3+}, $CaAl_2O_4$ (with Sr^{2+} in vacant Ca^{2+} sites) and $SrAl_2O_4$ are formed as major and minor phases, respectively.

The XRD spectrum for the S1 sample with $x = 0.7$ ($Sr_{0.3}Ca_{0.7}Al_2O_4$: 3 mol% Eu^{2+}, 1 mol% Dy^{3+}) is shown in Figure 11b. Unlike the $x = 0.5$ spectrum, the $x = 0.7$ spectrum did not contain $SrAl_2O_4$ peaks at 20.196° and 22.843°, suggesting that $CaAl_2O_4$ was formed homogeneously as the major phase. The primary $CaAl_2O_4$ peaks in Figure 11b were located at 29.878°, 35.326°, 37.045°, 60.138°, and 63.578°. Compared to the $CaAl_2O_4$ reference, these peaks are left-shifted by 0.410° on average. The gradual shifting behavior associated with raising the Ca^{2+} content from $x = 0.5$ to $x = 1.0$ was also observed in a study by Liu *et al.*[36] According to Liu *et al.*, this behavior was due to the expansion of the crystal lattice. When $x \geq 0.5$, $CaAl_2O_4$ was synthesized as the major phase of the material, and most (or all) of the Sr^{2+} ions were integrated into vacant Ca^{2+} sites in the matrix. Because the ionic radius of Sr^{2+} is greater than that of Ca^{2+}, the crystal lattice expanded when Sr^{2+} replaced Ca^{2+}, which caused a shift in the diffraction pattern. More Sr^{2+} ions promote a greater degree of lattice expansion; as a result, the shifts of the $Sr_{0.5}Ca_{0.5}Al_2O_4$: 3 mol% Eu^{2+}, 1 mol% Dy^{3+} diffraction peaks were greater than the $Sr_{0.3}Ca_{0.7}Al_2O_4$: 3 mol% Eu^{2+}, 1 mol% Dy^{3+} shifts.

The changes in crystal structure apparent in the XRD results are also exhibited by the emission spectra of the $Sr_{1-x}Ca_xAl_2O_4$:Eu^{2+}, Dy^{3+} series shown in Figure 12. The emissions in the Figure 12 spectra were produced by $4f^6 5d^1 \rightarrow 4f^7$ Eu^{2+} transitions discussed in Chapter I.

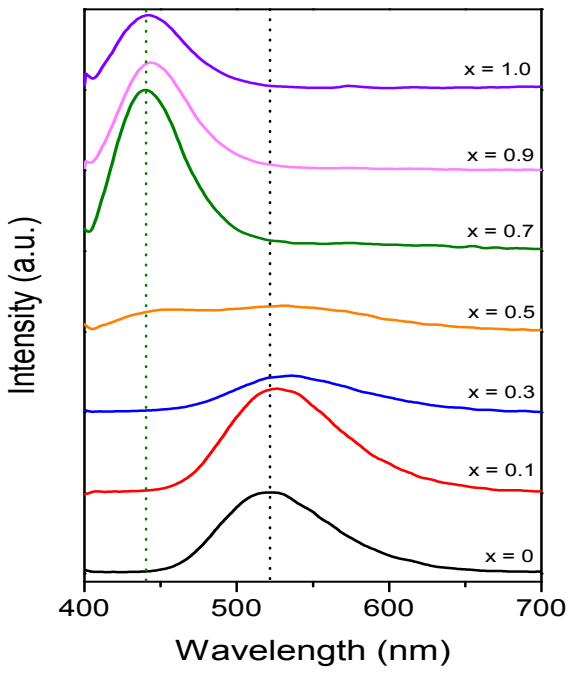

Figure 12. Stacked emission spectra of S1 phosphors, $Sr_{1-x}Ca_xAl_2O_4$: 3 mol% Eu^{2+}, 1 mol% Dy^{3+} (where x = 0, 0.1, 0.3, 0.5, 0.7, 0.9, and 1.0)

The $SrAl_2O_4$: 3 mol% Eu^{2+}, 1 mol% Dy^{3+} emission (shown in black in Figure 12) produced a broad peak, stretching from 450 nm to 650 nm and centered at 520 nm. The $CaAl_2O_4$: 3 mol% Eu^{2+}, 1 mol% Dy^{3+} emission spectrum (shown in purple in Figure 12) was narrower, stretching from 400 nm to 500 nm and centered at 445 nm. As the Ca^{2+} content was raised to x = 0.3 in $Sr_{1-x}Ca_xAl_2O_4$: 3 mol% Eu^{2+}, 1 mol% Dy^{3+}, a gradual red shift was observed—the x = 0.1 and x = 0.3 emission spectra were centered at 526 nm and 536 nm, respectively. This shift was likely due to slight distortion of the matrix caused by integrating Ca^{2+}, which has a smaller ionic radius than Sr^{2+}, into Sr^{2+} sites. The green emission of the $x \leq 0.3$ materials indicated that the major phase was $SrAl_2O_4$, because $SrAl_2O_4$: 3 mol% Eu^{2+}, 1 mol% Dy^{3+} emits in the green region of the visible spectrum. This is supported by the XRD data.

The $Sr_{0.5}Ca_{0.5}Al_2O_4$: 3 mol% Eu^{2+}, 1 mol% Dy^{3+} ($x = 0.5$) phosphor demonstrated a distinct change in emission color. The $x = 0.5$ emission spectrum in Figure 12 exhibited an extremely broad peak, stretching from 400 nm to 650 nm, with local maxima at ~440 nm and ~525 nm. The XRD data in Figure 11c suggested that $CaAl_2O_4$ was formed as the major phase when $x = 0.5$. There are three different crystallographic Ca^{2+} sites in $CaAl_2O_4$—two six-coordinated sites and one nine-coordinated site. Due to the relatively large radius of Eu^{2+}, Eu^{2+} ions at low concentrations tend to integrate into the larger 9-coordinated sites.[36] However, in $Sr_{0.5}Ca_{0.4}Al_2O_4$: 3 mol% Eu^{2+}, 1 mol% Dy^{3+}, three ions were competing for Ca^{2+} sites: Eu^{2+}, Dy^{3+}, and Sr^{2+}. Europium(II) and strontium(II), being similar in size, both preferred the 9-coordinated site; because of the relatively high concentration of Sr^{2+}, it is likely that many Eu^{2+} ions were forced into 6-coordinated sites. As was discussed in Chapter I, Eu^{2+}-based phosphor emissions change color based on the crystal field environment surrounding Eu^{2+}. Therefore, the blue emission of $Sr_{0.5}Ca_{0.5}Al_2O_4$: 3 mol% Eu^{2+}, 1 mol% Dy^{3+} was likely produced by Eu^{2+} ions in 9-coordinated sites, while the green emission was likely produced by Eu^{2+} ions in 6-coordinated sites.[36]

As the Ca^{2+} content increased from $x = 0.5$ to $x = 1.0$, the secondary 525 nm emission was no longer observed, and the 440 nm emission became more prominent in the spectrum. This was likely due to the decrease in Sr^{2+} content. With fewer Sr^{2+} ions to compete against, Eu^{2+} ions were easily integrated into nine-coordinated Ca^{2+} sites, consolidating the emission to ~440 nm.

To compare the emissions intensities of the phosphors from the S1 series,

$Sr_{1-x}Ca_xAl_2O_4$: 3 mol% Eu^{2+}, 1 mol% Dy^{3+}, overlapping emission spectra are shown in Figure 13. The emission spectra are normalized relative to the phosphor in the series that exhibited the greatest intensity.

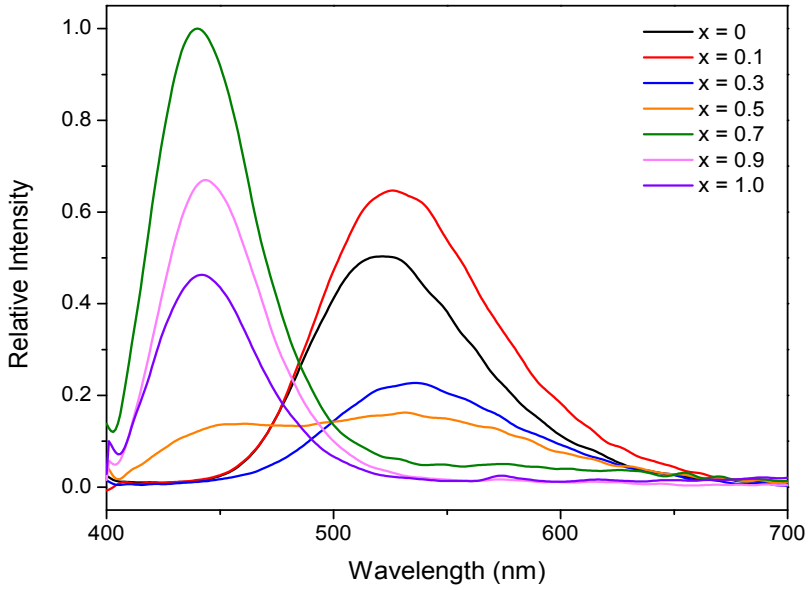

Figure 13. Overlapping emission spectra of S1 phosphors, $Sr_{1-x}Ca_xAl_2O_4$: 3 mol% Eu^{2+}, 1 mol% Dy^{3+} (where x = 0, 0.1, 0.3, 0.5, 0.7, 0.9, and 1.0)

Based on the emission spectra shown in Figure 13, the $Sr_{0.7}Ca_{0.3}Al_2O_4$: 3 mol% Eu^{2+}, 1 mol% Dy^{3+} (x = 0.7) phosphor produced the emission with the greatest measured intensity; thus, its y-value was normalized to 1. The $SrAl_2O_4$: 3 mol% Eu^{2+}, 1 mol% Dy^{3+} (x = 0) phosphor exhibited only ~50% of the counts-per-second that the x = 0.7 sample did at its respective peak wavelength. When the Ca^{2+} content was raised from x = 0 to x = 0.1, the emission intensity increased by 30%. This suggested that slight distortion of the $SrAl_2O_4$ phosphor matrix through Ca^{2+} integration can increase the brightness of the green $SrAl_2O_4$: 3 mol% Eu^{2+}, 1 mol% Dy^{3+} emission.

Increasing the Ca^{2+} content to $x = 0.5$ caused a significant drop in the emission intensity. According to the XRD data in Figure 11, $CaAl_2O_4$ was the major phase of $Sr_{0.5}Ca_{0.5}Al_2O_4$: 3 mol% Eu^{2+}, 1 mol% Dy^{3+}, and Sr^{2+} ions were incorporated into vacant Ca^{2+} sites, which forced Eu^{2+} ions into six-coordinated Ca^{2+} sites. Thus, the decreased emission intensity was likely caused by the distribution of Eu^{2+} ions into both six- and nine-coordinated sites. The total number of photons emitted by the $x = 0.5$ sample were split between two emissions—440 nm and 525 nm—which resulted in relatively low photon outputs in both regions.

At $x = 0.7$, the emission shifted completely into the blue region and the intensity reached a maximum within the S1 series. However, as Ca^{2+} content was raised from $x = 0.7$ to $x = 1.0$, the blue emission gradually decreased to ~45% of the $Sr_{0.3}Ca_{0.7}Al_2O_4$: 3 mol% Eu^{2+}, 1 mol% Dy^{3+} phosphor emission. This could have been due to a decrease in quantum efficiencies. A 2013 study by Luitel *et al.* determined that pure strontium aluminate phosphors exhibit up to 58% greater quantum efficiencies than their calcium counterparts, perhaps due to thermal energy losses in the latter. Thus, as Sr^{2+} incorporation decreased and the lattice shifted towards $CaAl_2O_4$, the photon output also decreased.

The full-width half maximum (FWHM) of $SrAl_2O_4$: 3 mol% Eu^{2+}, 1 mol% Dy^{3+} shown in Figure 13 was 83.02 nm. The FWHM of the sample with the greatest emission intensity, $Sr_{0.3}Ca_{0.7}Al_2O_4$: 3 mol% Eu^{2+}, 1 mol% Dy^{3+}, was 52.48 nm. The peaks with $SrAl_2O_4$ as the major phase ($x \leq 0.3$) were broad due to the presence of two distinct nine-coordinated sites for Eu^{2+} integration in the matrix.[18] Aside from $Sr_{0.5}Ca_{0.5}Al_2O_4$: 3 mol% Eu^{2+}, 1 mol% Dy^{3+}, the peaks with $CaAl_2O_4$ as the major phase were narrower; this is likely due to Eu^{2+} integration into a single nine-coordinated site rather than two. Thus, Eu^{2+} ions

integrate less discriminately into the two sites of the $SrAl_2O_4$ matrix, and the emitted photons vary more significantly in wavelength than those from the $CaAl_2O_4$ matrix. This is also exhibited in the excitation spectra for the S1 phosphors, shown in Figure 14.

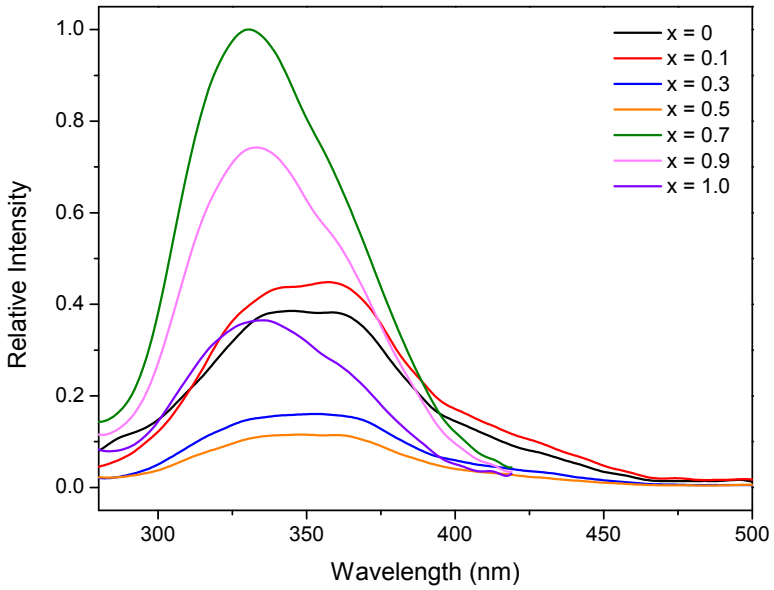

Figure 14. Excitation spectra of S1 phosphors, $Sr_{1-x}Ca_xAl_2O_4$: 3 mol% Eu^{2+}, 1 mol% Dy^{3+} (where x = 0, 0.1, 0.3, 0.5, 0.7, 0.9, 1.0)

The phosphors with $SrAl_2O_4$ as the major phase ($x \leq 0.3$) exhibited broad excitation peaks that plateaued from ~330 nm to ~375 nm before quickly tapering off to ~400 nm. These excitation spectra were likely composites of two separate excitation peaks—one for each nine-coordinated crystallographic site in the $SrAl_2O_4$ matrix. Because the two sites were energetically similar, the energies required to promote Eu^{2+} electrons from the $4f^7$ ground state to the $4f^6 5d^1$ excited state were also similar. This produces excitation peaks that overlap, as is shown in Figure 14. Similar overlapping was also observed in the $Sr_{0.5}Ca_{0.5}Al_2O_4$:

3 mol% Eu^{2+}, 1 mol% Dy^{3+} phosphor, due to the incorporation of Eu^{2+} ions into three distinct crystallographic Ca^{2+} sites.

The S1 phosphors with $x \geq 0.7$ produced much narrower excitation peaks centered at ~330 nm, with slight shoulders at ~360 nm. The shoulders corresponded to the crystal field splitting of the Eu^{2+} *d*-orbital.[13] It was apparent in Figures 12 and 13 that Eu^{2+} ions in $Sr_{0.3}Ca_{0.7}Al_2O_4$: 3 mol% Eu^{2+}, 1 mol% Dy^{3+}; $Sr_{0.1}Ca_{0.9}Al_2O_4$: 3 mol% Eu^{2+}, 1 mol% Dy^{3+}, and $CaAl_2O_4$: 3 mol% Eu^{2+}, 1 mol% Dy^{3+} were primarily incorporated into the nine-coordinated Ca^{2+} sites. Because Eu^{2+} ions were present in one distinct crystallographic site rather than two, the excitation peaks are narrower than those with $SrAl_2O_4$ as the major phase.

To determine which phosphor system to optimize, photos were taken of the S1 series under 365 nm excitation as well as after 5 s and 10 s intervals. The 365 nm excitation wavelength was chosen due to the widespread availability of 365 nm LED sources for practical applications of the phosphor ink. These images are shown in Figure 15.

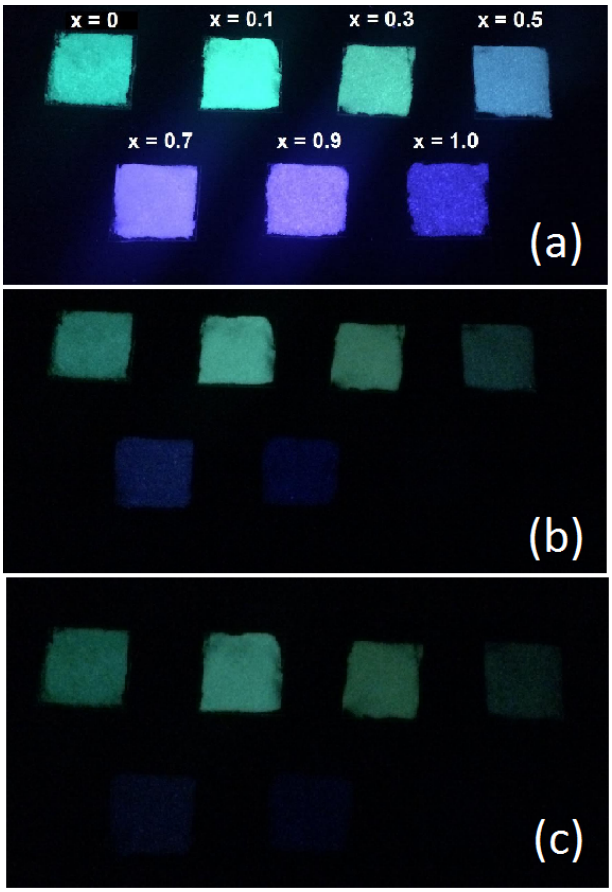

Figure 15. S1 phosphors (a) under 365 nm excitation, (b) 5 s after excitation, and (c) 10 s after excitation.

As the Ca^{2+} content increased from $x = 0$ to $x = 1.0$ in Figure 15, the phosphor emissions shifted from bright green to various shades of blue. This shift was also apparent in the S1 series emission spectra in Figures 12 and 13. However, it was evident in Figure 15 that the $SrAl_2O_4$ crystalline structure is better suited for Dy^{3+}-assisted persistent luminescence under 365 nm excitation, as the phosphors with $x \leq 0.3$ are much easier to detect with the naked eye at 10 s after excitation. This was also exhibited by the $Sr_{0.5}Ca_{0.5}Al_2O_4$: 3 mol% Eu^{2+}, 1 mol% Dy^{3+} phosphor. Although its emission under excitation appeared light blue, its green persistent luminescence suggested that the Eu^{2+} ions in the $SrAl_2O_4$ minor phase (shown in Figure 11c) were interacting with Dy^{3+} traps to extend the emission.

The difference in visibility between the blue- and green-emitting phosphors was also due to the respective locations of the colors on the visible spectrum. At ~440 nm, the blue emission was nearing the UV region. The 525 nm green emission was closer to the center of the visible region, where spectral sensitivity of the human eye is at a maximum. Furthermore, it is possible that the $CaAl_2O_4$ phosphors, $x = 0.7$, 0.9, and 1.0, could perform better if higher-energy excitation (e.g. 330 nm) was used, because 365 nm light may not be sufficient to excite the Eu^{2+} ions in the Ca^{2+} nine-coordinated sites. Thus, for potential applications where higher-energy excitation sources are available, the development of $CaAl_2O_4$:Eu^{2+}, Dy^{3+} phosphors may prove more promising.

Shown in Figures 13 and 15, partial substitution of the host ion for Sr^{2+} or Ca^{2+} can improve the emission intensity and persistent decay time for each respective phosphor system. However, despite the high measured emission intensity of $Sr_{0.7}Ca_{0.3}Al_2O_4$: 3 mol% Eu^{2+}, 1 mol% Dy^{3+} in Figure 13, $Sr_{0.9}Ca_{0.1}Al_2O_4$: 3 mol% Eu^{2+}, 1 mol% Dy^{3+} was chosen as the phosphor system to further optimize due to its practical visibility and luminescence lifetime under 365 nm excitation.

S2 Phosphor Series: Optimizing Eu^{2+} Dopant Content of $Sr_{0.9}Ca_{0.1}Al_2O_4$: x mol% Eu^{2+}, 1 mol% Dy^{3+}

Divalent europium(II) is the luminescence center of the $Sr_{0.9}Ca_{0.1}Al_2O_4$:Eu^{2+}, Dy^{3+} phosphor system. While long persistence—mainly a function of Dy^{3+}—is an important factor for the practical application of storage phosphors, a bright initial luminescence is essential for extending the luminescence lifetime, as it indicates a high degree of conduction band

population (and an increase in photons emitted). Thus, after selecting the most suitable Sr^{2+} to Ca^{2+} ratio, the Eu^{2+} content of $Sr_{0.9}Ca_{0.1}Al_2O_4$:Eu^{2+}, Dy^{3+} was optimized. In order to accomplish this, a series of $Sr_{0.9}Ca_{0.1}Al_2O_4$: *x* mol% Eu^{2+}, 1 mol% Dy^{3+} phosphors (where *x* = 0.01, 0.03, 0.05, 0.06, and 0.07) were synthesized and compared. The emission and excitation spectra of the S2 phosphor series are shown in Figure 16.

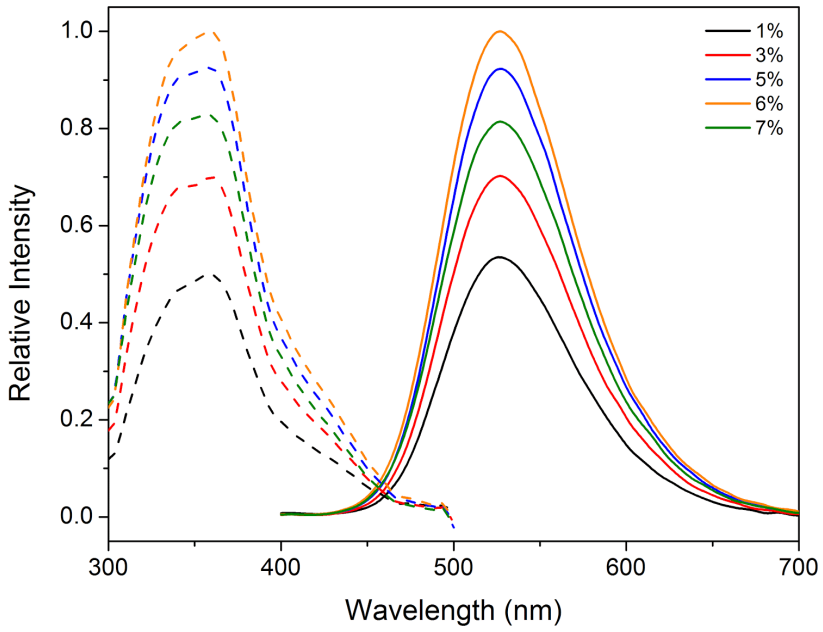

Figure 16. Excitation (dotted, λ_{em} = 525 nm) and emission (solid, λ_{ex} = 360 nm) spectra of S2 phosphors, $Sr_{0.9}Ca_{0.1}Al_2O_4$: *x* mol% Eu^{2+}, 1 mol% Dy^{3+} (where *x* = 1, 3, 5, 6, and 7)

It is important to note that, as shown in Figure 16, varying the Eu^{2+} content in the matrix does not affect the shape or location of the emission and excitation peaks of the material; the only significant change observed is the emission intensity. In the S1 phosphor series, the shape and location of the emission and excitation spectra changed with respect to Sr^{2+}/Ca^{2+} substitution, due to changes in the crystal field environment of Eu^{2+} ions. As is shown in Figure 16, as Eu^{2+} content of $Sr_{0.9}Ca_{0.1}Al_2O_4$: *x* mol% Eu^{2+}, 1 mol% Dy^{3+} approached

7 mol%, the crystal lattice was not altered. This was anticipated, because no major modification (>10 mol%) was occurring within the host matrix, as seen in the S1 phosphor series. However, this could also be due to the similar ionic radii of Sr^{2+} and Eu^{2+} ions—120 pm and 121 pm, respectively—which allowed Eu^{2+} to substitute for Sr^{2+} without significantly distorting the matrix.

In Figure 16, the emission intensity was lowest when Eu^{2+} content is 1 mol%, the lowest concentration in the sample series. Because Eu^{2+} was the emission center in the phosphor system, limiting Eu^{2+} ions in the crystal lattice limited the availability of photon-absorbing sites and, as a result, the amount of photons emitted at λ_{em} = 525 nm. It follows that the emission intensity increased as the concentration of Eu^{2+} increased to 6 mol%, for which it exhibited the maximum emission intensity in the series. When Eu^{2+} is increased to 7 mol%, a significant decrease in the intensity is observed. This is due to quenching of Eu^{2+}, which occurs when the ratio of host to dopant ions is too small for a given phosphor system.[9] Thus, the $Sr_{0.9}Ca_{0.1}Al_2O_4$: 6 mol% Eu^{2+}, 1 mol% Dy^{3+} storage phosphor system was chosen for further optimization.

S3 Phosphor Series: Optimizing Dy^{3+} Dopant Content of $Sr_{0.9}Ca_{0.1}Al_2O_4$: 6 mol% Eu^{2+}, x mol% Dy^{3+}

Trivalent dysprosium(III), an auxiliary activator in the crystal lattice[6], was primarily responsible for the persistent luminescence of the phosphor material. The substitution of Dy^{3+} for Sr^{2+} in the crystal lattice—which propagates in a manner similar to Eu^{2+}—creates energy "traps" that populate the conduction band over time.[21] This was shown in the

luminescence decay curves by Matsuzawa *et al.* (Figure 1). $SrAl_2O_4$:Eu^{2+}, Dy^{3+} exhibited a brighter luminescence and longer emission lifetime than $SrAl_2O_4$:Eu^{2+} by an order of magnitude.[11] Other trivalent lanthanide ions, such as Nd^{3+}, Er^{3+}, and Ce^{3+} have been shown to increase the intensity and duration of the emission when incorporated as co-dopants in a strontium aluminate phosphor[20,34,35]; these ions also create electron traps of similar depths to Dy^{3+} traps that also populate the combustion band by thermal recombination.[35] However, Dy^{3+} was chosen as a co-dopant for this phosphor material due to its small ionic radius, which allows it to substitute easily into 9-coordinated sites in both the $SrAl_2O_4$ and $CaAl_2O_4$ matrices as well as 6-coordinated sites in the $CaAl_2O_4$ matrix.[35] To optimize the Dy^{3+} content in the matrix, a series of $Sr_{0.9}Ca_{0.1}Al_2O_4$: 6 mol% Eu^{3+}, *x* mol% Dy^{3+} (where *x* = 0.01, 0.03, 0.05, and 0.07) were synthesized by CST; the emission and excitation spectra of this series are shown in Figure 17.

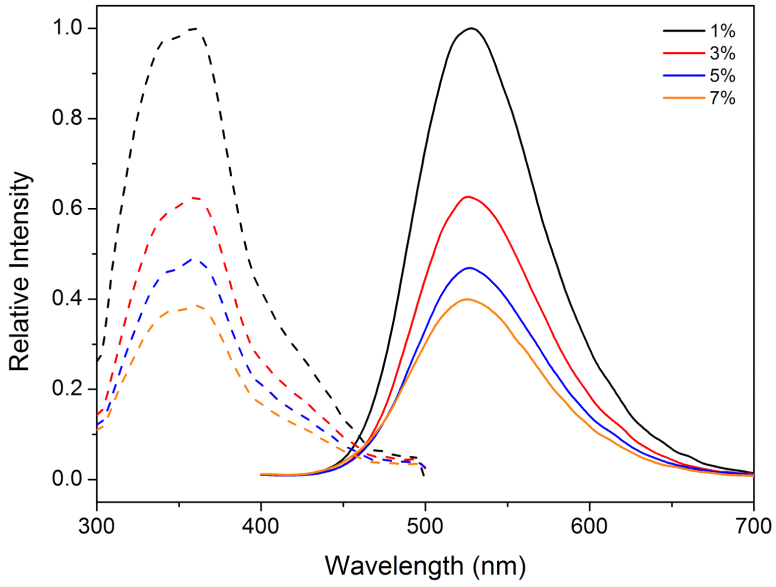

Figure 17. Excitation (dotted, λ_{em} = 525 nm) and emission (λ_{ex} = 360 nm) spectra of S3 phosphors, $Sr_{0.9}Ca_{0.1}Al_2O_4$: 6 mol% Eu^{2+}, *x* mol% Dy^{3+} (where *x* = 1, 3, 5, and 7)

As the Dy^{3+} content increased from 1 mol% to 7 mol% in the $Sr_{0.9}Ca_{0.1}Al_2O_4$: 6 mol% Eu^{2+}, *x* mol% Dy^{3+} phosphor system (S3 phosphor series), the emission ($\lambda_{ex} = 360$ nm) and excitation ($\lambda_{em} = 525$ nm) spectra of the materials gradually decreased in intensity. The $Sr_{0.9}Ca_{0.1}Al_2O_4$: 6 mol% Eu^{2+}, 1 mol% Dy^{3+} storage phosphor produced the brightest emission in the series.

Although the emission and excitation spectra (Figure 17) did not suggest a shift in phase due to their relatively consistent location and shape, the emission peak for $Sr_{0.9}Ca_{0.1}Al_2O_4$: 6 mol% Eu^{2+}, 7 mol% Dy^{3+} exhibited a slight blue shift compared to the peaks with 1, 3, and 5 mol% Dy^{3+}. With a combined dopant concentration of 13 mol% (6 mol% Eu^{2+} and 7 mol% Dy^{3+}), the decreased emission intensity was indicative of the low host to dopant ion ratio. The blue shift was most likely another effect of the host to dopant ion ratio; the increased competition among Ca^{2+}, Eu^{2+}, and Dy^{3+} for vacant Sr^{2+} integration sites in the matrix increased the likelihood that Eu^{2+} and Ca^{2+} ions would fill sites within close proximity of one another. It was shown in the S1 phosphor series that, as the Ca^{2+} content was raised in $Sr_{1-x}Ca_xAl_2O_4$: 3 mol% Eu^{2+}, 1 mol% Dy^{3+}, the emission spectra of the material exhibited strong blue shifts (Figure 12). This could be an indication that raising the Ca^{2+} content in the host matrix caused a crystal-field splitting (non-degeneracy) to occur with the Eu^{2+} 5*d* and 4*f* orbitals. It follows that in the $Sr_{0.9}Ca_{0.1}Al_2O_4$: 6 mol% Eu^{2+}, 7 mol% Dy^{3+} crystal lattice, in which 10 mol% Ca^{2+}, 6 mol% Eu^{2+}, and 7 mol% Dy^{3+} ions were incorporated into Sr^{2+} sites, some Eu^{2+} ions were subject to Ca^{2+}-influenced crystal field splitting and a slight blue shift occurred.

S4 Phosphor Series: Optimizing the Eu^{2+}:Dy^{3+} Ratio of $Sr_{0.9}Ca_{0.1}Al_2O_4$: (7-x) mol% Eu^{2+}, x mol% Dy^{3+}

In Figure 17, the $Sr_{0.9}Ca_{0.1}Al_2O_4$: 6 mol% Eu^{2+}, 1 mol% Dy^{3+} demonstrated the greatest intensity within the S3 phosphor series. However, as seen in Figure 16, the luminescence intensity of $Sr_{0.9}Ca_{0.1}Al_2O_4$: *x* mol% Eu^{2+}, 1 mol% Dy^{3+} storage phosphors with 1 to 7 mol% Eu^{2+} content shows the performance of the material is quenched when Eu^{2+} was 7 mol% (for a combined dopant concentration of 8 mol%). In order to confirm that lowering the ratio of Eu^{2+} to Dy^{3+} in the phosphor system resulted in a decrease in emission intensity rather than caused a decrease due to quenching, a series of phosphors was synthesized with a constant combined dopant concentration of 7 mol% in which the ratio of Eu^{2+} to Dy^{3+} was varied (S4 phosphor series). The emission spectrum of this series is shown in Figure 18.

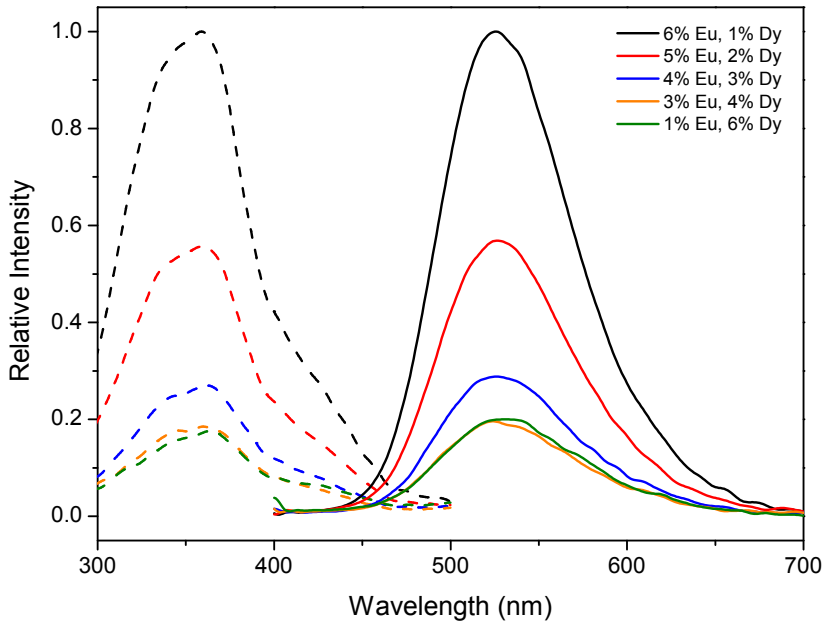

Figure 18. Excitation (dotted, λ_{em} = 525 nm) and emission (solid, λ_{ex} = 360 nm) spectra of

S4 phosphors, $Sr_{0.9}Ca_{0.1}Al_2O_4$:(7 – *x*) mol% Eu^{2+}, *x* mol% Dy^{3+} (where *x* = 1, 2, 3, 4, and 6)

Five phosphors with a 7 mol% dopant concentration were synthesized with Eu^{2+} to Dy^{3+} ratios of 6:1, 5:2, 4:3, 3:4, and 1:6. In Figure 18, as the Eu^{2+}:Dy^{3+} ratio shifted to favor Dy^{3+}, the emission intensity of the phosphor material also decreased until reaching a constant intensity for 3:4 and 1:6. This suggested that quenching of the matrix was not the sole cause of emission intensity loss in Figure 17, as decreasing Eu^{2+} content by as little as 1 mol% and increasing Dy^{3+} content by 1 mol% while holding the overall dopant content constant results in a significant loss in intensity.

An optimal Eu^{2+} to Dy^{3+} dopant ratio of 6:1 does not align with the findings of other studies of $SrAl_2O_4$:Eu^{2+}, Dy^{3+} phosphors. For example, multiple studies found an optimal Eu^{2+}:Dy^{3+} ratio of 1:2.[9,13,38] This discrepancy could be the result of crystal matrix distortion by Ca^{2+} or differences in phase resulting from the respective synthesis methods. Thus, while this study suggested a greater density of Eu^{2+} luminescence centers produces a brighter emission, others have produced phosphors that improve in emission intensity with higher concentrations of auxiliary activators.

It was not determined in this study if the phosphors with greater Dy^{3+} content exhibited longer luminescence lifetimes than those favoring Eu^{2+}. In this case, low emission intensity for any phosphor with $x \geq 2$ mol% compared to $Sr_{0.9}Ca_{0.1}Al_2O_4$: 6 mol% Eu^{2+}, 1 mol% Dy^{3+} was sufficient to assume that any gain in persistence would not overcome the loss of practical applicability caused by the dull emission. Thus, the $Sr_{0.9}Ca_{0.1}Al_2O_4$: 6 mol% Eu^{2+}, 1 mol% Dy^{3+} phosphor was chosen for further optimization.

S5 Phosphor Series: Optimizing H_3BO_3 Flux of $Sr_{0.9}Ca_{0.1}Al_2O_4$: 6 mol% Eu^{2+}, 1 mol% Dy^{3+}, x *mol% H_3BO_3*

In order to lower the required reaction temperature to ensure complete synthesis, decrease particle size, and facilitate the integration of Eu^{2+} ions into the matrix[26], a flux material was incorporated into the $Sr_{0.9}Ca_{0.1}Al_2O_4$: 6 mol% Eu^{2+}, 1 mol% Dy^{3+} combustion process. Boric acid, H_3BO_3, has been demonstrated as a suitable flux material for $SrAl_2O_4$:Eu^{2+}, Dy^{3+} phosphors, improving both the emission intensity and luminescence lifetime of the materials.[24] To determine the effect of H_3BO_3 addition on $Sr_{0.9}Ca_{0.1}Al_2O_4$: 6 mol% Eu^{2+}, 1 mol% Dy^{3+}, a series of phosphors with $Sr_{0.9}Ca_{0.1}Al_2O_4$: 6 mol% Eu^{2+}, 1 mol% Dy^{3+}, *x* mol% H_3BO_3, where *x* = 0, 10, 15, 20, 30, and 40, were synthesized. The emission spectra of these phosphors are shown in Figure 19.

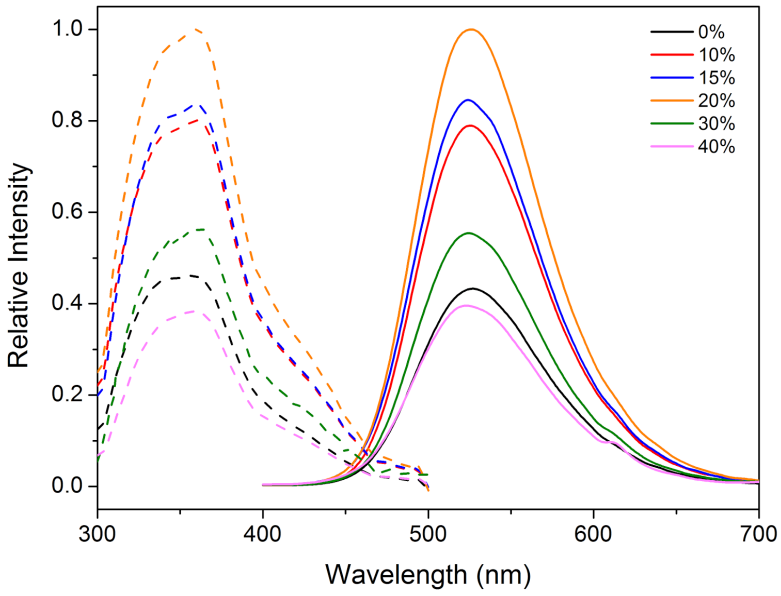

Figure 19. Excitation (dotted, λ_{em} = 525 nm) and emission (solid, λ_{ex} = 360 nm) spectra of S5 phosphors, $Sr_{1-x}Ca_xAl_2O_4$: 6 mol% Eu^{2+}, 1 mol% Dy^{3+}, *x* mol% H_3BO_3 (where *x* = 0, 10, 15, 20, 30, and 40)

It was evident in Figure 19 that incorporation of ≤30 mol% H_3BO_3 during synthesis improved the emission intensity of the phosphor. Adding 10 mol% H_3BO_3 (*x* = 10) doubled the emission intensity versus not including H_3BO_3 (*x* = 0). The series reached a maximum emission intensity at 20 mol% H_3BO_3 before decreasing rapidly at 30 mol% and 40 mol%. According to Nag and Kutty, when the B_2O_3 content (formed from H_3BO_3 during synthesis) is sufficiently high, O—Al—O—Al bonds in the aluminate framework are broken and O—B—O—Al bonds are formed, causing the formation of strontium borate or strontium aluminoborate glass. However, the phosphors studied by Nag and Kutty were synthesized by SSRT; the behavior of H_3BO_3 during combustion could differ due to the rapid rate of reaction. The current study in agreed with the results of Wang *et al.*, who determined $SrAl_2O_4$:Eu^{2+}, Dy^{3+} phosphors synthesized by CST with 19 mol% H_3BO_3 exhibit maximum emission intensity. Furthermore, Wang *et al.* observed a blue shift in samples with >20 mol% H_3BO_3—potentially due to the substitution of B^{3+} ions into Al^{3+} sites as hypothesized by Nag *et al.*—which is also shown in Figure 19 for 30 mol% and 40 mol% H_3BO_3.

To examine the effect of H_3BO_3 addition on the size and morphology of the $Sr_{0.9}Ca_{0.1}Al_2O_4$: 6 mol% Eu^{2+}, 1 mol% Dy^{3+} phosphor particles, SEM images of the S5 phosphors with 0 mol% and 20 mol% H_3BO_3 were taken. The SEM images for the phosphors synthesized without H_3BO_3 are shown in Figure 20.

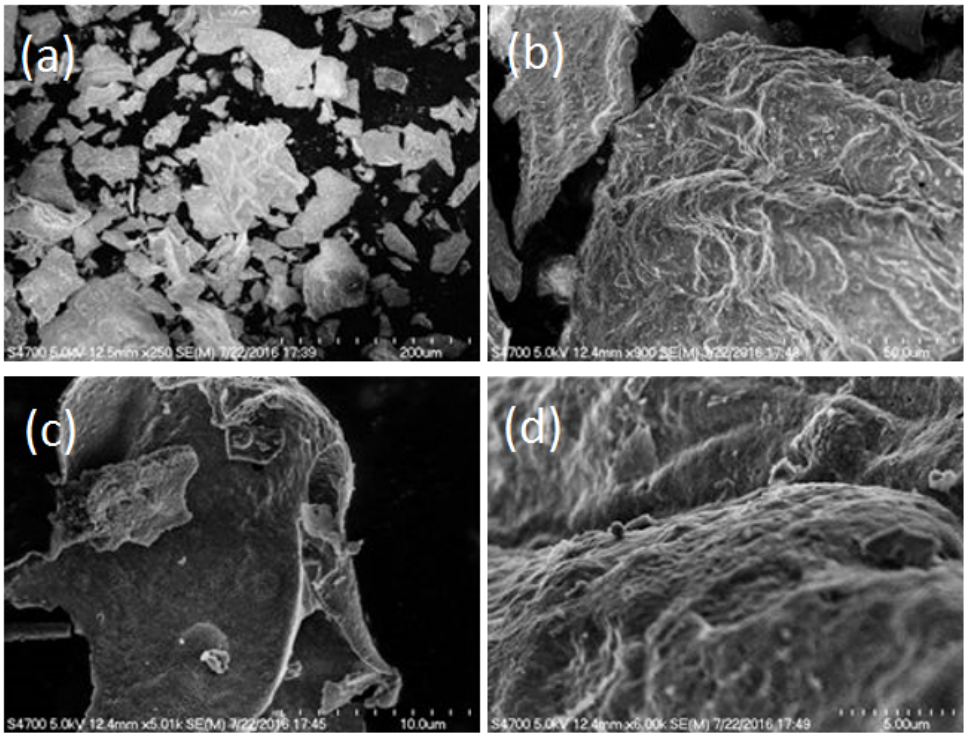

Figure 20. SEM images of $Sr_{0.9}Ca_{0.1}Al_2O_4$: 6 mol% Eu^{2+}, 1 mol% Dy^{3+}, 0 mol% H_3BO_3 at different resolutions: (a) 200 μm scale, (b) 50 μm scale, (c) 10 μm scale, and (d) 5 μm scale.

Figure 20a depicts an overall representation of the phosphor particles, which were hundreds of micrometers in size. The particles are irregular in shape and exhibit a wide-range particle size distribution, which is a direct result of the exothermic combustion process. In Figure 20d, sub-micron particles were seen on the surface of the phosphor material. Nanocrystalline $SrAl_2O_4$:Eu^{2+}, Dy^{3+} storage phosphors have been synthesized by CST.[9] Thus, it could be that under the given synthesis parameters, a relatively small amount of $SrAl_2O_4$:Eu^{2+},Dy^{3+} nanoparticles are produced alongside the larger micron particles. Fracture lines are visible in Figure 20a, suggesting that smaller particles may have melted together during synthesis to form the micron-sized product; it is possible that mechanical stress caused by ultrasonic vibration or physical grinding could break the particles at these fracture lines to produce smaller materials.

The SEM images of $Sr_{0.9}Ca_{0.1}Al_2O_4$: 6 mol% Eu^{2+}, 1 mol% Dy^{3+}, 20 mol% H_3BO_3 are shown in Figure 21.

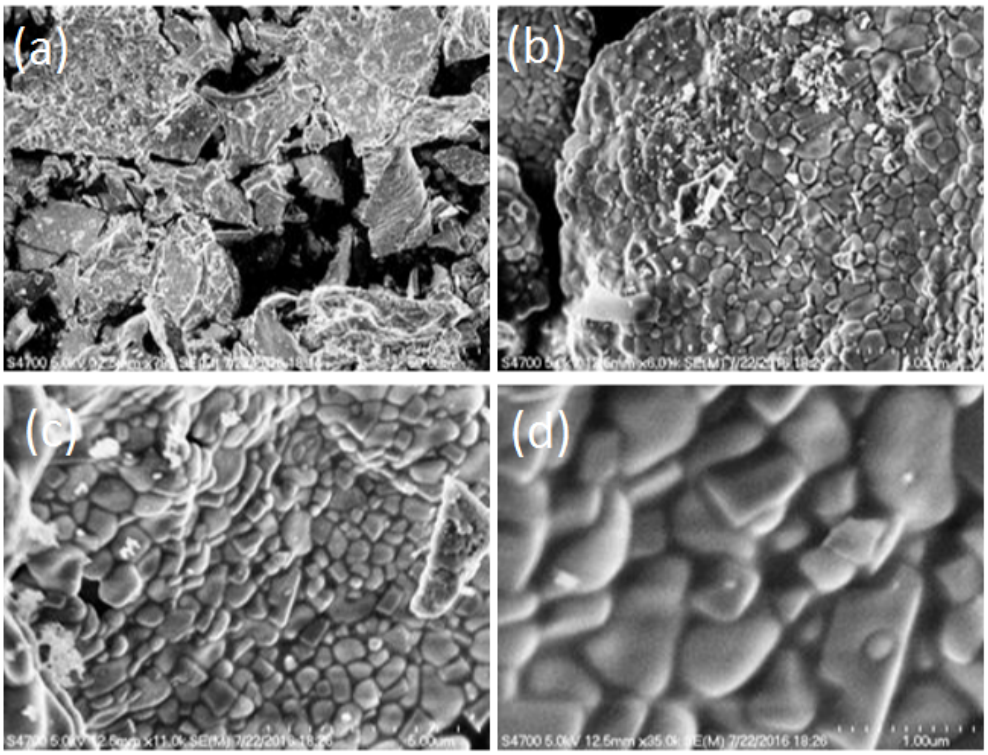

Figure 21. SEM images of $Sr_{0.9}Ca_{0.1}Al_2O_4$: 6 mol% Eu^{2+}, 1 mol% Dy^{3+}, 20 mol% H_3BO_3 at different resolutions: (a) 50 µm scale, (b) 5 µm scale, (c) 5 µm scale, and (d) 1 µm scale.

The shape of the particles synthesized with H_3BO_3 in Figure 21a resembled those shown in Figure 20a; they were plate-shaped particles many hundreds of micrometers in size. However, the surface of the phosphor material synthesized with H_3BO_3 (Figure 21b-d) differed significantly from the material synthesized without a flux. The bulk phosphor material was an agglomeration of smaller particles; given the 1.00 µm scale of Figure 21d, it was apparent the smaller particles were submicron in size. This change in surface morphology was also observed by Nag and Kutty, who postulated that H_3BO_3 flux both lowers the activation energy of the reaction and accelerates the recrystallization of

$SrAl_2O_4:Eu^{2+}$, Dy^{3+} grains, causing the partial melting of phosphor particles after the rapid initial synthesis process. If the H_3BO_3 content were higher, it is likely that the strontium aluminoborate glass phase would appear in the SEM images.

Although bulk, micron-sized phosphors are suitable for some applications, such as safety signage, ceramics, and solar cells, colloidal ink solutions for phosphor printing typically requires nanosized phosphor materials.[5] Thus, development of an ink solution with the $Sr_{0.9}Ca_{0.1}Al_2O_4$: 6 mol% Eu^{2+}, 1 mol% Dy^{3+} phosphor material would require a reduction in particle size. It is possible that certain changes in the synthesis method, such as reducing the extent of particle melting, could produce nanophosphors. Various post-treatments—such as ultrasonic vibration, agate grinding, or ball milling—could also be investigated for reducing the phosphor particle size, as enough applied stress could cause breakage at the interparticle fracture lines and reverse the effect of melting. However, nanophosphor materials have been shown to produce less intense emissions than their micron counterparts, and excessive mechanical stress is shown to decrease the effectiveness of the phosphor, perhaps due to the introduction of surface defects in the material.[9,14] The incorporation of H_3BO_3 could partially prevent such effects; not only does it increase the emission intensity of the phosphor material, it also produces phosphors with more apparent interparticle fracture boundaries that would likely take less stress to break into nanoparticles than those synthesized without flux.

Luminescence Decay of Optimized Phosphor Material

To quantify the luminescence lifetime of $Sr_{0.9}Ca_{0.1}Al_2O_4$: 6 mol% Eu^{2+}, 1 mol% Dy^{3+}, 20 mol% H_3BO_3, a luminescence decay curve was collected after the phosphor material was excited for 10 minutes by 365 nm light. The decay curve is shown in Figure 22.

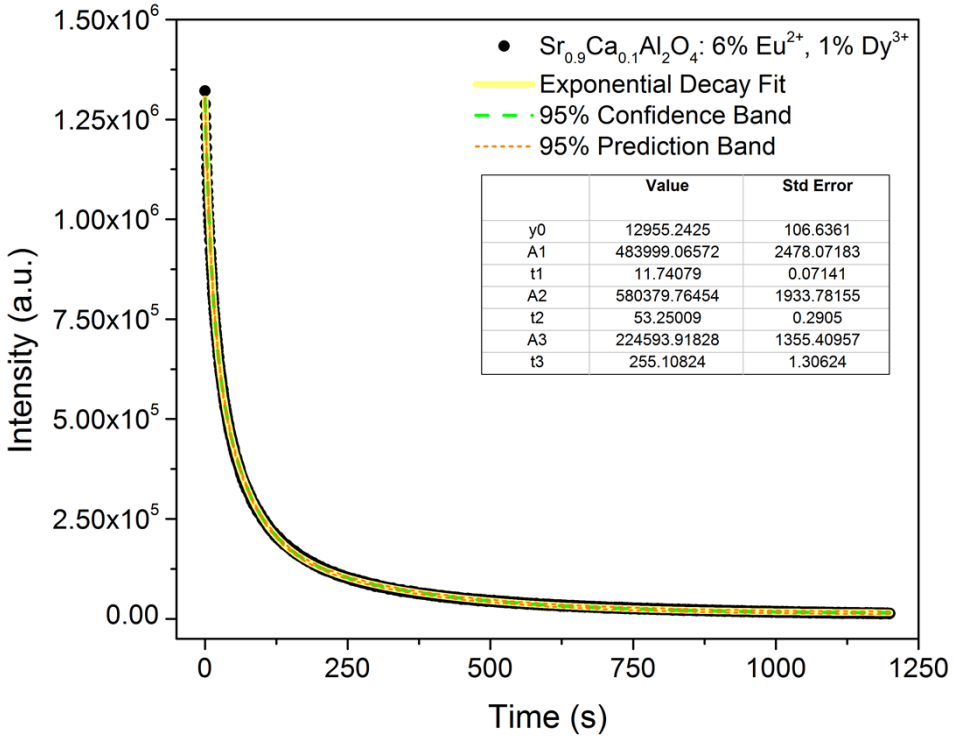

Figure 22. Luminescence decay curve of $Sr_{0.9}Ca_{0.1}Al_2O_4$: 6 mol% Eu^{2+}, 1 mol% Dy^{3+}, 20 mol% H_3BO_3 after 10 minutes under λ_{ex} = 365 nm

The decay curve in Figure 22 was modeled as a third-order exponential decay, following the general formula:

$$I = A_1 e^{\left(\frac{-t}{\tau_1}\right)} + A_2 e^{\left(\frac{-t}{\tau_2}\right)} + A_3 e^{\left(\frac{-t}{\tau_3}\right)}$$

where I is the phosphorescence intensity, A_n are constants, t is time and τ_n are decay times for the fast (τ_1), intermediate (τ_2), and slow (τ_3) components of the luminescence decay.[39] The exponential fit curve for the $Sr_{0.9}Ca_{0.1}Al_2O_4$: 6 mol% Eu^{2+}, 1 mol% Dy^{3+}, 20 mol% H_3BO_3 phosphor was as follows:

$$1.2955 \times 10^4 = 4.8400 \times 10^5 e^{\left(\frac{-t}{11.741\ s}\right)} + 5.8038 \times 10^5 e^{\left(\frac{-t}{53.250\ s}\right)} + 2.2459 \times 10^5 e^{\left(\frac{-t}{255.11\ s}\right)}$$

The fast, intermediate, and slow emissions lasted for approximately 11.74 s, 53.25 s, and 255.11 s, respectively, for a total observed lifetime of ~320 s. These values were similar to luminescence lifetimes observed for other phosphor systems.[39] However, because the fluorometer used for this collection was not capable of pulse excitation, there could be slight error in modeling—particularly of the rapid initial decay. There is a necessary delay as the shutter closes and the excitation source is removed from the sample path, and it is possible that the first few seconds of luminescence decay are not recorded as a result. The luminescence lifetime collected by the fluorometer could also be extended by lengthening the period of excitation or increasing the detector slit width. Furthermore, the detection limit of the fluorometer detector does not correspond directly to the detection limit of the naked eye; thus, the practical luminescence lifetime for field applications could differ from that which is reported in this study. As a result, the luminescence decay model would be most useful for comparing the $Sr_{0.9}Ca_{0.1}Al_2O_4$: 6 mol% Eu^{2+}, 1 mol% Dy^{3+}, 20 mol% H_3BO_3 phosphor lifetime to other similar candidates under identical conditions.

Future Work and Development

In this study, the emission intensity and luminescence lifetime of the popular $SrAl_2O_4:Eu^{2+}$, Dy^{3+} phosphor system were enhanced by partial substitution of Ca^{2+} into Sr^{2+} sites in the matrix. The $Sr_{0.9}Ca_{0.1}Al_2O_4$ phosphor host was then optimized for Eu^{2+} and Dy^{3+} dopant content as well as the extent of H_3BO_3 flux addition during synthesis. The resulting phosphor, $Sr_{0.9}Ca_{0.1}Al_2O_4$: 6 mol% Eu^{2+}, 1 mol% Dy^{3+}, 20 mol% H_3BO_3, was a viable candidate for further development of a colloidal phosphor ink solution due to its improved emission intensity and luminescence lifetime compared to the unoptimized system (Figures 13 and 15).

However, the $Sr_{0.9}Ca_{0.1}Al_2O_4$: 6 mol% Eu^{2+}, 1 mol% Dy^{3+}, 20 mol% H_3BO_3 phosphors synthesized in this study were hundreds of micrometers in size, which is generally too large for printing applications due to the parameters of the delivery system (i.e., the size of the ink delivery apparatus). Therefore, future work on this phosphor system could include the incorporation of an ultrasonic vibration, agate grinding, or ball milling post-treatment technique to facilitate breakage at the interparticle fracture lines shown in Figure 21, producing nanoparticles from the micron-sized agglomerates. Further studies on this phosphor system should also include a more robust investigation of the persistent luminescence of the material and, if necessary, alteration of the synthesis method or incorporation of another dopant ion to extend it. Also, it may be useful to further characterize and investigate the final phosphor material in order to better understand its structural and optical characteristics relative to potential applications.

APPENDIX 1: FLUOROMETER DATA SPECIFICATIONS

Figures 12 and 13

To produce the emission spectra shown in Figures 12 and 13, $Sr_{1-x}Ca_xAl_2O_4:Eu^{2+}$, Dy^{3+} phosphors with x = 0, 0.1, and 0.3 were excited with 360 nm light. Phosphors with x = 0.5 and 0.7 were excited at 350 nm, and phosphors with x = 0.9 and 1.0 were excited at 330 nm.

Figure 14

To produce the excitation spectra shown in Figure 14, the emissions of $Sr_{1-x}Ca_xAl_2O_4:Eu^{2+}$, Dy^{3+} phosphors with x = 0, 0.1, 0.3, and 0.5 were measured at 520 nm, 526 nm, 534 nm, and 536 nm, respectively. The emissions of phosphors with x = 0.7, 0.9, and 0.1 were measured at 440 nm.

WORKS CITED

[1]Kaur, J.; Shrivastava, R.; Jaykumar, B.; Suryanarayana, N. S. Studies on the Persistent Luminescence of Eu^{2+} and Dy^{3+}-doped $SrAl_2O_4$ Phosphors: A Review. *Res. Chem. Intermed.* **2014**, *40*, 317-343.

[2]Robinson, J. W.; Skelly Frame, E. M.; Frame, G. M. II. *Undergraduate Instrumental Analysis*, 7th ed.; CRC: Boca Raton, FL, 2014.

[3]Singh, D.; Tanwar, V.; Samantilleke, A. P.; Mari, B.; Bhagwan, S.; Singh Kadyan, P.; Singh, I. Preparation and Photoluminescence Properties of $SrAl_2O_4$:Eu^{2+}, RE^{3+} Green Nanophosphors for Display Device Applications. *J. Electron. Mater.* **2016**, *45* (6), 2718-2724.

[4]Rojas-Hernandez, R. E.; Rodriguez, M. A.; Fernandez, J. F. Role of the Oxidizing Agent to Complete the Synthesis of Strontium Aluminate Based Phosphors by the Combustion Method. *RSC Adv.* **2015**, *5*, 3104-3112.

[5]Rojas-Hernandez, R. E.; Rodriguez, M. A.; Rubio-Marcos, F.; Serrano, A.; Fernandez, J. F. Designing Nanostructured Strontium Aluminate Particles with High Luminescence Properties. *J. Mater. Chem. C* **2015**, *3*, 1268-1276.

[6]Shin, H.; Ullah, S.; Chung, K. Effect of Nominal Substitution of Dy^{3+} for Host Cations in $SrAl_2O_4$:Eu^{2+} Phosphor on Phase Evolution and Long Afterglow Luminescence. *J. Alloys Compd.* **2012**, *544*, 181-187.

[7]Peng, T.; Yang, H.; Pu, X.; Hu, B.; Jiang, Z.; Yan, C. Combustion Synthesis and

Photoluminescence of $SrAl_2O_4$:Eu,Dy Phosphor Nanoparticles. *Mater. Lett.* **2004**, *58*, 352-356.

[8]Atabaev, T. S.; Hwang, Y. H.; Kim, H. K. Color-Tunable Properties of Eu^{3+}-and-Dy^{3+}-Codoped Y_2O_3 Phosphor Particles. *Nanoscale Res. Lett.* **2012**, *7* (1), 556-562.

[9]Kshatri, D. S.; Khare, A. Comparative Study of Optical and Structural Properties of Micro- and Nanocrystalline $SrAl_2O_4$:Eu^{2+}, Dy^{3+} Phosphors. *J. Lumin.* **2014**, *155*, 257-268.

[10]Harvey, E. N. *A History of Luminescence: From the Earliest Times Until 1900;* The American Philosophical Society: Philadelphia, 1957.

[11]Matsuzawa, T.; Aoki, Y.; Takeuchi, N.; Murayama, Y. A New Long Phosphorescent Phosphor with High Brightness, $SrAl_2O_4$:Eu^{2+}, Dy^{3+}. *J. Electrochem. Soc.* **1996**, *143*, 2670-2673.

[12]Van den Eeckhout, K.; Poelman, D.; Smet, P. F. Persistent Luminescence in Non-Eu^{2+}-Doped Compounds: A Review. *Materials* **2013**, *6*, 2789-2818.

[13]Bem, D. B.; Swart, H. C.; Luyt, A. S.; Duvenhage, M. M.; Dejene, F. B. Characterization of Luminescent and Thermal Properties of Long Afterglow $SrAl_xO_y$:Eu^{2+}, Dy^{3+} phosphor synthesized by combustion method. *Polym. Compos.* **2011**, *32* (2), 219-226.

[14]Chander, H.; Haranath, D.; Shanker, V.; Sharma, P. Synthesis of Nanocrystals of Long Persisting Phosphor by Modified Combustion Technique. *J. Cryst. Growth* **2004**, *271*, 307-312.

[15]McQuarrie, D. A.; Simon, J. D. *Physical Chemistry: A Molecular Approach*; University Science: Sausalito, 1997.

[16]Katsumata, T.; Sasajima, K.; Nabae, T.; Komuro, S.; Morikawa, T. Characteristics of

Strontium Aluminate Crystals Used for Long-Duration Phosphors. *J. Am. Ceram. Soc.* **1998**, *81* (2), 413-416.

[17]Haranath, D.; Shanker, V.; Chander, H.; Sharma, P. Tuning of Emission Colors in Strontium Aluminate Long Persisting Phosphor. *J. Phys. D. Appl. Phys.* **2003**, *36*, 2244-2248.

[18]Swati, G.; Chawla, S.; Mishra, S.; Rajesh, B.; Vijayan, N.; Sivaiah, B.; Dhar, A.; Haranath, D. Investigation on luminescence enhancement and decay characteristics of long afterglow nanophosphors for dark-vision display applications. *Appl. Surf. Sci.* **2015**, *333*, 178-185.

[19]Qiu, Z.; Zhou, Y.; Lü, M.; Zhang, A.; Ma, Q. Combustion Synthesis of Long-Persistence Luminescent $MAl_2O_4:Eu^{2+}$, RE^{3+} (M = Sr, Ba, Ca, R = Dy, Nd, and La) Nanoparticles and Luminescence Mechanism Research. *Acta. Mater.* **2007**, *55*, 2615-2620.

[20]Shanker, V.; Haranath, D.; Swati, G. Persistence Mechanisms and Applications of Long Afterglow Phosphors. *Def. Diff. Forum* **2015**, *361*, 69-94.

[21]Zhong, H.; Zeng, X. Preparation of MAl_2O_4: Eu^{2+}, Sm^{3+} (M = Ca, Sr, Ba) Phosphors by the Combustion Method and Their Luminescent Properties. *S. Afr. J. Chem.* **2008**, *61*, 22-25.

[22]Dutczak, D.; Jüstel, T.; Ronda, C.; Meijerink, A. Eu^{2+} Luminescence in Strontium Aluminates. *Phys. Chem. Chem. Phys.* **2015**, *7*, 15236-1524.

[23]Terraschke, H.; Wickleder, C. UV, Blue, Green, Yellow, Red, and Small: Newest Developments on Eu^{2+}-Doped Nanophosphors. *Chem. Rev.* **2015**, *115*, 11352-11378.

[24]Nag, A.; Kutty, T.R.N. Role of B_2O_3 on the Phase Stability and Long Phosphorescence of $SrAl_2O_4$:Eu,Dy. *J. Alloys. Compd.* **2003**, *354*, 221-231.

[25]Wang, H.F.; Xing, G.Z.; Wang, X. Y.; Bati, X. G.; Zhang, L.; Li, S. Tailoring Photoluminescence in Strontium Aluminate Phosphors Using Fluxing Agent and Activators: Rational Synthesis via a Facial Microwave-Assisted Method. *Mater. Sci. Semicond. Process.* **2014**, *27*, 1007-1012.

[26]Haranath, D.; Sharma, P.; Chander, H.; Ali, A.; Bhalla, N.; Halder, S. K. Role of Boric Acid in Synthesis and Tailoring the Properties of Calcium Aluminate Phosphor. *Mater. Chem. Phys.* **2007**, *101*, 163-169.

[27]Son, N. M.; Thao Vien, L. T.; Khoa Bao, L. V.; Trac, N. N. Synthesis of $SrAl_2O_4:Eu^{2+}$, Dy^{3+} Phosphorescence Nanosized Powder by Combustion Method and its Optical Properties. *J. Phys.: Conf. Ser.* **2009**, *187*(1), 1-6.

[28]Mothudi, B. M.; Ntwaeaborwa, O. M.; Botha, J. R.; Swart, H. C. Photoluminescence and Phosphorescence Properties of $MAl_2O_4:Eu^{2+}$, Dy^{3+} (M = Ca, Ba, Sr) Phosphors Prepared at an Initiating Combustion Temperature of 500℃. *Physica B* **2009**, *404*, 4440-4444.

[29]Suriyamurthy, N.; Panigrahi, B. S. Effects of Non-Stoichiometry and Substitution on Photoluminescence and Afterglow Luminescence of $Sr_4Al_{14}O_{25}:Eu^{2+}$, Dy^{3+} Phosphor. *J. Lumin.* **2008**, *128*, 1809-1814.

[30]Luitel, H. M.; Watari, T.; Chand, R.; Torikai, T.; Yada, M. Giant Improvement on the Afterglow of $Sr_4Al_{14}O_{25}:Eu^{2+}$, Dy^{3+} Phosphor by Systematic Investigation on Various Parameters. *J. Mat.* **2013**, 1-10.

[31]Yu, X.; Zhou, C.; He, X.; Peng, Z.; Yang, S-P. The \Influence of Some Processing

Conditions on Luminescence of $SrAl_2O_4:Eu^{2+}$ Nanoparticles Produced by Combustion Method. *Mater. Lett.* **2004**, *58* (6), 1087-1091.

[32]Dacyl, D.; Uhlich, D.; Jüstel, T. The Effect of Calcium Substitution on the Afterglow of Eu^{2+}/Dy^{3+}-Doped $Sr_4Al_{14}O_{25}$. *Cent. Eur. J. Chem.* **2009**, *7* (2), 164-167.

[33]Wu, Q.; Liu, Z.; Jiao, H. Luminescent Properties of Stabled Hexagonal Phase $Sr_{1-x}Ba_xAl_2O_4:Eu^{2+}$ ($x = 0.37 – 0.70$). *Physica B* **2009**, *404*, 2499-2502.

[34]Yu, N.; Liu, F.; Li, X.; Pan, Z. Near Infrared Long-Persistent Phosphorescence in $SrAl_2O_4:Eu^{2+}$, Dy^{3+}, Er^{3+} Phosphors Based on Persistent Energy Transfer. *Appl. Phys. Lett.* **2009**, *95*, 231110.

[35]Lakshmanan, A. *Luminescence and Display Phosphors: Phenomena and Applications*; Nova Science: New York, 2008.

[36]Liu, C.; Wang, Y.; Hu, Y.; Chen, R.; Liao, F. Adjusting Luminescence Properties of $Sr_{1-x}Ca_xAl_2O_4$: Eu^{2+}, Dy^{3+} Phosphors by Sr/Ca Ratio. *J. Alloys. Compd.* **2009**, *470*, 473-476.

[37]Luitel, H. M.; Watari, T.; Chand, R.; Torikai, T.; Yada, M.; Mizukami, H. Tuning the Luminescence Color and Enhancement of Afterglow Properties of $Sr_{(4-x-y-)}Ca_xBa_yAl_{14}O_{25}$: Eu^{2+},Dy^{3+} Phosphor by Adjusting the Composition. *Mater. Sci. Eng. B* **2013**, 834-842.

[38]Han, S-D.; Singh, K.C.; Cho, T-Y.; Lee, H-S.; Jakhar, D.; Hulme, J.P.; Han, C-W.; Kim, J-D.; Chun, I-S.; Gwak, J. Preparation and Characterization of Long Persistence Strontium Aluminate Phosphor. *J. Lumin*. **2008**, *128*(3), 301-305.

[39]Kshatri, D.S.; Khare, A. Characterization and Optical Properties of Dy^{3+} Doped Nanocrystalline $SrAl_2O_4:Eu^{2+}$ Phosphor. *J. Alloys Compd.* **2014**, *588*, 499-495.